UC-403
LBL-27879

Lawrence Berkeley Laboratory
UNIVERSITY OF CALIFORNIA

EARTH SCIENCES DIVISION

Presented at the NATO Advanced Study Institute on Transport Processes in Porous Media, Pullman, WA, July 9–18, 1989, and to be published in the Proceedings

Fluid Flow in Fractured Rock: Theory and Application

J.C.S. Long, K. Hestir, K. Karasaki, A. Davey, J. Peterson, J. Kemeny, and M. Landsfeld

July 1989

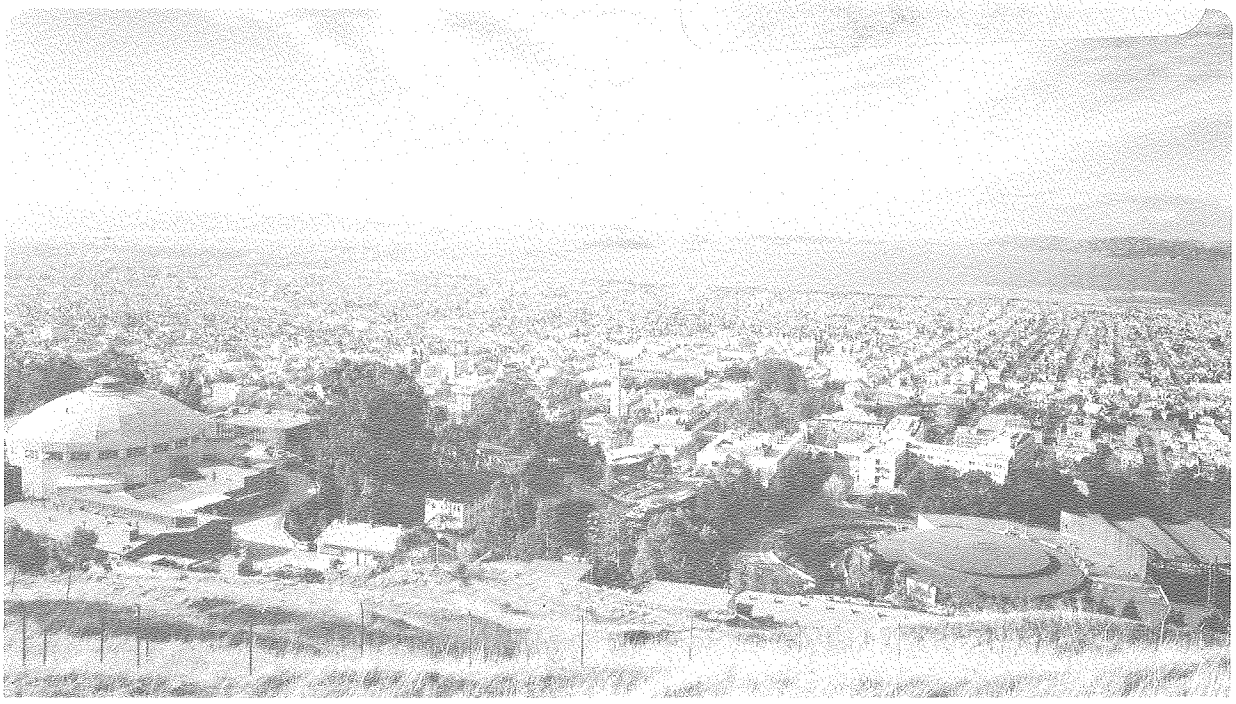

Prepared for the U.S. Department of Energy under Contract Number DE-AC03-76SF00098.

LBL-27879

Fluid Flow in Fractured Rock: Theory and Application

J. C. S. Long, K. Hestir, K. Karasaki,
A. Davey, J. Peterson, J. Kemeny, and M. Landsfeld.

Earth Sciences Division
Lawrence Berkeley Laboratory
1 Cyclotron Road
Berkeley, California 94720

July 1989

This work was supported by the Manager, Chicago Operations, Repository and Technology Program, of the U.S. Department of Energy, under Contract No. DE-AC03-76SF00098.

To be published in *Transport Processes in Porous Media,*
J. Bear and M. Y Corapcioglu, eds.,
Kluwer Academic Publishers,
The Netherlands

FLUID FLOW IN FRACTURED ROCK: THEORY AND APPLICATION

J. C. S. Long, K. Hestir, K. Karasaki, A. Davey, J. Peterson, J. Kemeny and M. Landsfeld
Earth Sciences Division
Lawrence Berkeley Laboratory
1 Cyclotron Road
Berkeley, CA

ABSTRACT. The phenomena of fluid flow in fractured rock is dominated by the fact that is not all parts of the domain are in hydraulic communication. In theory, it is possible to determine connectivity and permeability from stochastic parameters that describe the fracture geometry. When this approach is applied to the field we find it very difficult to sufficiently determine the geometry which controls the flow. Simulated annealing, an inverse technique which focus on finding the pattern of conductors may provide a better way to characterize these systems.

1. Introduction

In cases where the matrix rock can be considered impermeable, fluid flow in fractured rock is controlled by the geometry of the fracture network. If the fractures are not interconnected, then flow will not occur. If they are highly interconnected, then fluid flow in the rock will resemble fluid flow in a porous media. Between these two extremes, the flow system will be complex and can not necessarily be treated as an equivalent continuum.

This paper examines the problem of representing the fracture network with an equivalent flow system. Numerical techniques are used to examine how the fracture geometry determines how the system can be represented as an equivalent continuum. In particular we use equivalent media theory to look at how connectivity (or the degree of interconnection) in a network controls the permeability. The obvious next step is to try to determine fracture geometry in the field and use this information to predict the hydrologic behavior. Experience with this approach has shown that there are major difficulties in learning enough about the fracture geometry to define the hydrologic behavior.

How can we then develop models of these partially connected fracture systems? We need to somehow represent the fact that the fracture network is partially connected without requiring all the details of the geometry. A new approach is under development which blends information from geology, geophysics and hydrology in an inverse method designed to determine a percolation lattice which behaves the same way that the real system is observed to behave. An example application of this idea is described as the last part of this paper.

2. Theoretical Studies

We can easily study the way in which geometry of a fracture network controls the hydrologic behavior using numerical models and a simple conceptual model for the fractures. For example, we have looked at two-dimensional systems where we assume the "fractures" are one-dimensional, finite line segments. In

other words, two-dimensional pipe networks. In fact, this may not be a bad model for three-dimensional fracture networks if most of the conductance is in the intersections between fractures or the flow in the fractures is channelized.

We next must decide some rules about how to put the fracture "pipes" on the plane, and how to distribute their length, orientation and conductivity. Further, we may decide on rules for truncating fractures where they intersect other fractures. Given these rules, realizations of hypothetical fracture networks can be generated. For each realization, we know the conductivity of each pipe and how the pipes are connected. Therefore, we can use a simple algorithm to calculate flow in the pipe network under any boundary conditions we wish to apply. If necessary, we could create many realizations of the same statistical system at the same scale to determine how variable the flow systems might be. More importantly, we can see how the statistical parameters which control the generation of the network control the hydrologic behavior.

Studies of this type have been done by Robinson (1984), Dershowitz (1984), Long (1983), and Long and Witherspoon (1985). Most recently Hestir and Long (1989) have looked at a limited class of these models called Poisson models, and developed an analytical expression for permeability as a function of the statistical parameters controlling the generation of the network. This work is discussed here.

The Poisson model is one of the simplest models for two-dimensional fracture networks (Long et al., 1982). In this model, the fractures which are line segments are located in the plane using a Poisson process. Practically, this means that we choose a square region of a specified size, L x L and pick x- and y-coordinates for a specified number of line centers from a uniform distribution, U[0,L]. Next, we choose the orientation distribution for the lines. This can be any distribution. The lines are then assigned lengths according to a length distribution and finally conductance is assigned to each line. In the cases described here, all fractures are assigned the same conductance. Fractures are truncated at the boundaries of the region, but no other truncation rules are applied to the fractures.

For given statistical parameters, we can generate fracture networks and then calculate their permeability. Parameter studies can be designed to determine the effect of the statistical parameters and the effect of scale of measurement on the permeability. It turns out that these studies are a member of a class of problems known as percolation problems or equivalent media problems. Percolation and equivalent media theories therefore provide the basis for developing an analytical expression for permeability and the scale of the Representative Elementary Volume (REV).

2.1. PERCOLATION THEORY AND EQUIVALENT MEDIA THEORY

Percolation theory and equivalent media theory are usually applied to problems on regular lattices (e.g. Figures 2.1a-d). Two types of problems can be defined: bond percolation or site percolation. In either case, percolation theory and equivalent media theory describe the equivalent permeability of the lattices as the bonds or sites are randomly filled with probability, p.

The amount of literature covering percolation problems is massive and one author points out that the number of publications per year is growing exponentially. Perhaps the most important reason for this that the relationships derived from percolation theory are largely heuristic. There is a small but growing body of mathematical proof to support such conclusions (Kesten, 1987). However, it is mostly the weight of evidence from numerical studies that leads to the belief that these relationships are valid. Percolation problems are often studied with a Monte Carlo approach. For a given value of p, realizations of lattices of a given size are created and their properties studied. The expected value of permeability, K, of such systems is a function of p and the size of the lattice used, i.e., scale of measurement.

As p increases, clusters of bonds or sites are formed and these clusters increase in size with increases in p. At the critical probability, p_{crit}, at least one cluster suddenly becomes infinite in size in what is called a critical phenomenon. Percolation theory looks at the conductance of these lattices when $p \approx p_{crit}$. Equivalent media theory is applied to cases where p is significantly larger than p_{crit}.

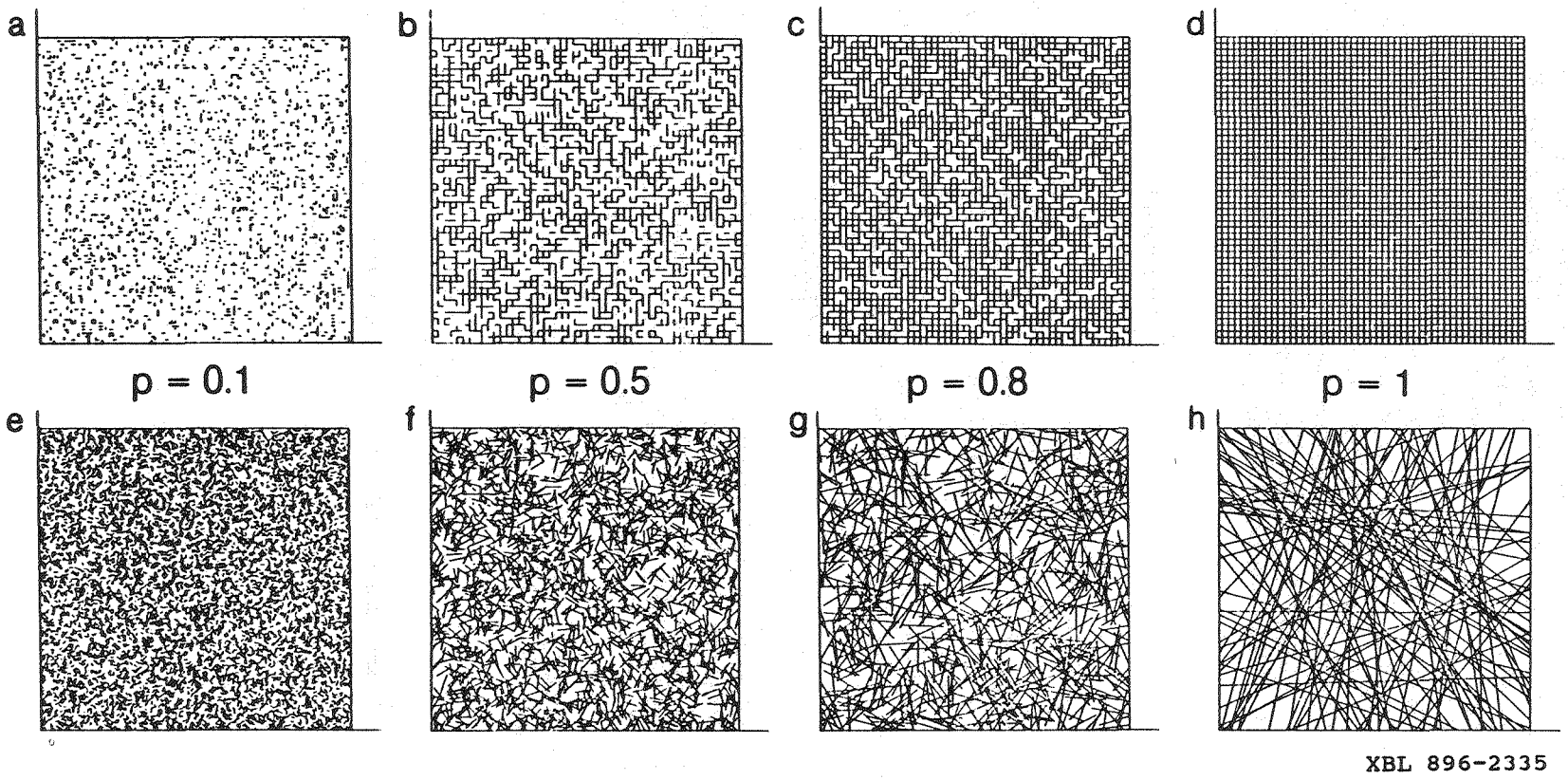

Figure 2.1. Examples of percolating networks: (a) through (d) are regular lattices which correspond to the random Poisson networks (e) through (h) below them.

If we could observe these systems on an infinite scale, percolation theory tells us that we could immediately tell whether the value of p was above or below critical. Above critical, the lattice would be percolative (or conductive), i.e., have at least one infinite cluster. Below critical, all clusters would be finite in size. However, we can only observe at finite scales. At finite scales some conductive graphs will be created even when $p < p_{crit}$. Also, for some cases that are above critical, the realization will not be conductive. As we increase the scale of measurement we should find that the frequency of conductive realizations decreases for systems that are below critical. On the other hand if the system is above critical, increases in scale will increase the percolation frequency. An estimate of p_{crit} is often made by finding the value of p for which the percolation frequency at any finite scale is 0.5 (Englman et al., 1983).

As p increases, K increases. Relationships between p and K have been deduced through Monte Carlo studies. From percolation literature, Orbach (1985) for example gives for $p \approx p_{crit}$ in bond percolation:

$$\frac{K}{K_{p=1}} \propto (p-p_{crit})^t \tag{2.1}$$

where $K_{p=1}$ is the permeability at $p = 1$.

For most two-dimensional bond percolation on regular lattices, p_{crit} depends on the particular lattice and is between about 0.35 to 0.65. The exponent t is considered to be a universal constant, i.e. it is independent of the lattice type. Monte Carlo results usually indicate that t is about 1.1 but various calculations have t between 1.1 and 1.3.

A second important relationship is for ξ, the scale on which homogeneous behavior is observed. In hydrology, we call ξ the "REV". Orbach gives this relationship as:

$$\xi \propto C\left|p-p_{crit}\right|^{-\nu} \tag{2.2}$$

where ν is thought to be exactly 4/3 for two-dimensional systems and C is a constant which is of the order of the lattice element. Between the scale of C and ξ the medium has fractal properties in that similar looking clusters of lattice elements occur on all scales. Because Equations (1) and (2) are conjectures based on numerical study the symbol "$\propto$" is loosely defined and can be read as "goes as". It can mean anything from the ratio of the two sides tends to 1 to the ratio of the logarithms of the two sides tends to one (Kesten 1982).

From the equivalent media literature, Kirkpatrick (1973) for example, one can find another relationship between K and p for the case where $p > p_{crit}$:

$$\frac{K}{K_{p=1}} = 1 - \frac{(1-p)}{(1-2/z)} \tag{2.3}$$

where z is the coordination number defined as the number of bonds coordinated with a site. For example, on a square lattice, z is four. This expression predicts a linear relationship between p and K. Kirkpatrick supports this relationship with perturbation analysis of the matrix equation for values of potential in the lattice.

In summary we have:

(1) Permeability on the infinite scale becomes non-zero at $p > p_{crit}$

(2) For $p > p_{crit}$ permeability initially increases exponentially in $p-p_{crit}$ (percolation theory) and then becomes linear in p (equivalent media theory) for constant values of coordination number, z.

(3) The REV increases exponentially as p approaches p_c.

2.2. PERCOLATION AND EQUIVALENT MEDIA THEORIES APPLIED TO FRACTURE NETWORK

In applying these theories to fracture networks we must resolve the following problems: What is p and what is z? The probability, p, is well defined for a lattice problem. In any given lattice it can be simply estimated by dividing the number of bonds (or sites) present by the total number available to fill. In random fracture networks it is not so clear what p is. Likewise, the definition of coordination number, z, is clear on a regular lattice. On a random system it may be that z is not an integer.

In percolation problems on a lattice, an upper bound for conductivity exists for the case where $p = 1$. When all the lattice elements are filled (Figure 2.1d). For any case of $p \leq 1$, the resulting permeability can be normalized against the case of $p = 1$. Thus the normalized permeability will be 1 when $p = 1$. For random fracture networks, there is theoretically no end to the degree of fracturing. Each time a fracture is added to the system, the permeability increases *ad infinitum*. For fracture systems considered in this manner, there is no upper bound on permeability and it would be difficult to normalize the results of parameter studies. In other words, the fracture system which corresponds to the lattice with $p = 1$ is difficult to identify. As there is no obvious case which represents a "completely filled" lattice, we cannot determine how "relatively filled" a fracture network is.

We have solved the problem of defining p for a random system by comparing systems which have the same linear fracture frequency, λ_l (the number of fractures that intersect a line of length unity corrected for orientation bias). This way of looking at the system turns out to be the key to finding p. If λ_l is fixed, then the permeability of the fracture network will be a maximum if the fractures are infinite in length. This, in fact, is exactly the case studied by Snow (1965, 1969) where the fracture frequency was known from borehole observations and Snow made the assumption that the fractures were infinite in length. Thus Snow's permeability can be taken as the permeability equivalent to the lattice case where $p = 1$.

The fact that Snow's permeability is an upper bound can be seen through heuristic arguments. Consider a two-dimensional Poisson network of line segments with random orientations given by the probability density function rate, $f(\phi)$. The Poisson process of fracture centers has rate, λ_A and the average line length is $\bar{l}$. The rate of line segment intersections on a given reference line (i.e. a borehole) is $\tilde{\lambda}_l$. Terzaghi (1965) gave the relationship between these parameters as

$$\tilde{\lambda}_l = \bar{l}\,\lambda_A\, E(\cos\phi) \ ,$$

where ϕ is the angle between the poles of the fractures and the borehole and

$$E(\cos\phi) = \int_0^{\frac{\pi}{2}} \cos\phi f(\phi) d\phi \ .$$

A line frequency corrected for orientation can be defined by:

$$\lambda_l = \frac{\tilde{\lambda}_l}{E(\cos\phi)} \ .$$

which simplifies the above relationship to

$$\lambda_l = \bar{l}\lambda_A \ , \tag{2.4}$$

The quantity λ_l is equivalent to the average linear fracture frequency when all fractures are perpendicular to the borehole, i.e. as if $\phi = 0$ for all fractures. The value of λ_l can be calculated from borehole data using the observed fracture frequency and the orientation of the fractures relative to the borehole.

From Equation 2.4 it can be seen that a variety of systems which all have the same λ_l can be constructed by increasing the mean length of the fractures, $\bar{l}$, by the same factor that the number of fractures per unit area, λ_A is decreased or visa versa. In other words, a system with a lot of short fractures and a system with a few long fractures look the same from the borehole.

Now to see that Snow's permeability is an upper bound we suppose that we have a two dimensional system of dimension LxL with $\lambda_A L^2$ lines of finite length $l < L$. To build a system with the same λ_l and a higher permeability we can rearrange the same lines such that they have the same λ_l in the following way. Place the lines end to end to form one line of length L_0. Clearly, $L_0 = l\,\lambda_A L^2$. Now break this long line into N lines of length L where $N = L_0/L$ and for convenience suppose that N is an integer so that we can do this evenly. Stack these N fractures in parallel across the medium so they look "infinite" in length because they transect the entire LxL region (Figure 2.2). Let the line rate of the rearranged system be λ_l'. λ_l' is equal to λ_l because

$$\lambda_l' = \frac{N}{L} = \frac{L_0}{L^2} = \frac{L^2 \lambda_A l}{L^2} = \lambda_A l = \lambda_l.$$

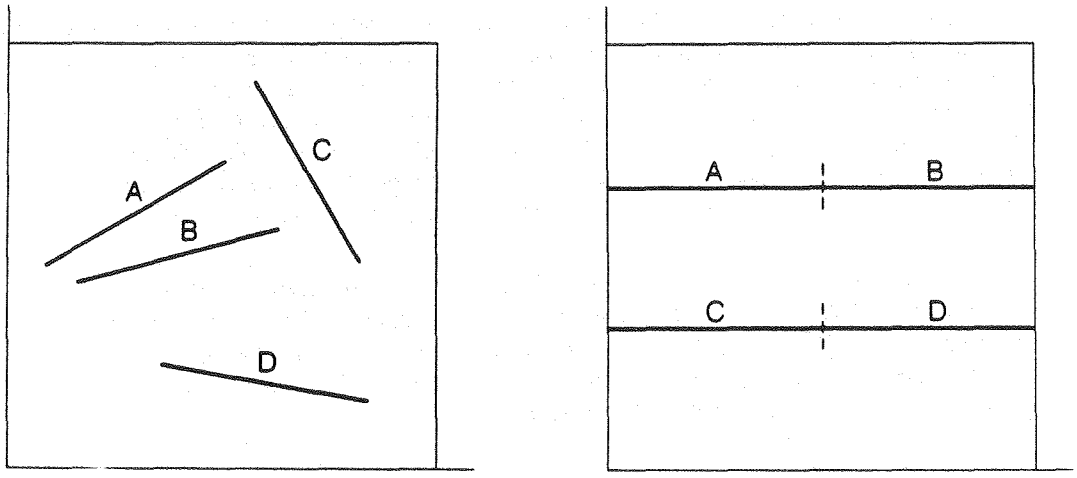

XBL 888-10395

Figure 2.2. Rearranging fractures such that they appear "infinite".

Obviously this is the most efficient way to arrange lines for flow so the average permeability (K_S) of this rearranged "Snow" system must be an upper bound. These arguments also imply that the directionally averaged Snow's permeability only depends on λ_l:

$$K_S = k_0 \lambda_l \tag{2.5}$$

where k_0 is a constant that depends on units and the conductance of the line segments.

As we have found a way to define a maximum permeability, our work is reduced to finding a relationship between the parameters which control the geometry of the network and p and z such that the observed permeabilities can be explained with percolation and equivalent media theories. This we do in three steps. First, we derive an expression for connectivity, ζ, in terms of the geometric parameters. Then, we propose relationships between connectivity and p and connectivity and z. Finally, we use our parameter studies conducted with constant λ_l to verify that the proposed expressions for p yields relationships for permeability which fit Equations 2.1 and 2.3.

2.3. A MEASURE OF CONNECTIVITY

Several authors have used the average number of intersections per fracture, ζ, as a measure of the connectivity in a random line processes (Robinson, 1984, and Charlaix et al., 1986). In this section we give ζ as a function of the statistical parameters governing the network and describe a few of its properties as shown in Hestir and Long (1989).

Let $f(l)$ denote the probability density function for line length and let $g(\theta)$ denote the probability density function for orientation. We assume that line orientation, length and placement are statistically independent and we take $0 \le \theta < \pi$ and θ measured counter clockwise from horizontal. Choose a particular line segment of length l_0 and orientation θ_0. The expected number of segments intersecting this line is:

$$= \lambda_A l_0 \bar{l} \int_0^{\pi} \sin\left|\theta_0 - \theta\right| g(\theta) d\theta$$

where

$$\bar{l} = E(l) = \int_0^{\infty} l f(l) dl \ .$$

To randomize l_0 and θ_0 we take an average over all values of θ_0 and l_0. This gives:

$$\zeta = \lambda_A (\bar{l})^2 \int_0^{\pi}\int_0^{\pi} \sin\left|\theta_0 - \theta\right| g(\theta) g(\theta_0) d\theta d\theta_0 \ .$$

We can write this equation as:

$$\zeta = \lambda_A (\bar{l})^2 H(\Theta) \tag{2.6}$$

where

$$H(\Theta) = \int_0^{\pi}\int_0^{\pi} \sin\left|\theta_0 - \theta\right| g(\theta) g(\theta_0) d\theta d\theta_0 \ .$$

We will call $H(\Theta)$ the orientation correction factor. We give two examples of values of $H(\Theta)$ for different orientation distributions. When Θ is uniformly distributed on $[\,0\,,\,\pi\,]$ ie., $g(\theta) = 1/\pi$, then

$$H(\Theta) = \frac{2}{\pi} \ .$$

For two orthogonal sets of lines of equal frequency we don't have a probability density but we can still evaluate the integral taking $g(\theta) = \frac{1}{2}\delta(\theta) + \frac{1}{2}\delta(\theta - \frac{\pi}{2})$ where δ is the dirac delta function. This yields:

$$H(\Theta) = \frac{1}{2} \ .$$

We have shown that ζ is directly proportional to $\lambda_A(\bar{l})^2$. There is a nice heuristic reason for this that follows from the fact that ζ is a dimensionless quantity. The reasoning goes like this. Let λ_A be the areal rate of line centers as used above. A natural thing to do is to rescale the line system so that the average line length is one. Let λ_A^N be the area rate of line centers in the in the rescaled system; we will call this the normalized density. One easily shows that $\lambda_A^N = \lambda_A(\bar{l})^2$. So ζ is proportional to the normalized density which we can intuitively relate to connectivity.

To study cases with varying ζ we note that

$$\zeta = \lambda_A(\bar{l})^2 H(\Theta) = \lambda_l \bar{l} H(\Theta)$$

So we can vary ζ and still keep λ_L constant. For example in Figures 2.1 e-h, we increase $\bar{l}$ by the same proportion that we decrease λ_A. As l approaches infinity, λ_l remains constant but ζ increases, and the permeability approaches the limiting case described by Snow (1965) (Figure 2.1h). Further, as any value of λ_l can be rescaled to any other value, studying any one value of λ_l should allow one to predict permeability for any other value.

2.4. A FUNCTIONAL FORM FOR K/K_S

In this section we present a functional form for normalized permeability, K/K_S. This requires finding expressions for p and z in terms of ζ. This expression is substituted into Eqn. (2.1) or (2.3) to obtain an expression for K/K_S in terms of ζ. We test this functional form against numerical studies. The expression is not a mathematical fact but rather a guess based on analogues with other systems. Similar work has been presented by Robinson (1984) and Englman et al. (1983). However Hestir and Long (1989) have shown that these other models do not work as well for variable fracture length cases.

We find p as a function of ζ by finding the average length of a line in the regular lattice bond model as a function of p and the average length of a line in the random line model as a function of ζ then equating the two averages. First consider the bond percolation model where p is defined as the probability that a particular bond is present. Think of a given existing bond as a piece of a line in a random line system (Figure 2.3a). Let b denote this bond. To make b a piece of a line which is k bonds long we would have to attach a total of $k-1$ bonds to b followed by no bonds on the ends. This can be done a total of k different ways each with probability $p^{k-1}(1-p)^2$. Thus the probability that b is in a line k bonds long is

$$kp^{k-1}(1-p)^2 \quad k = 1,2,...$$

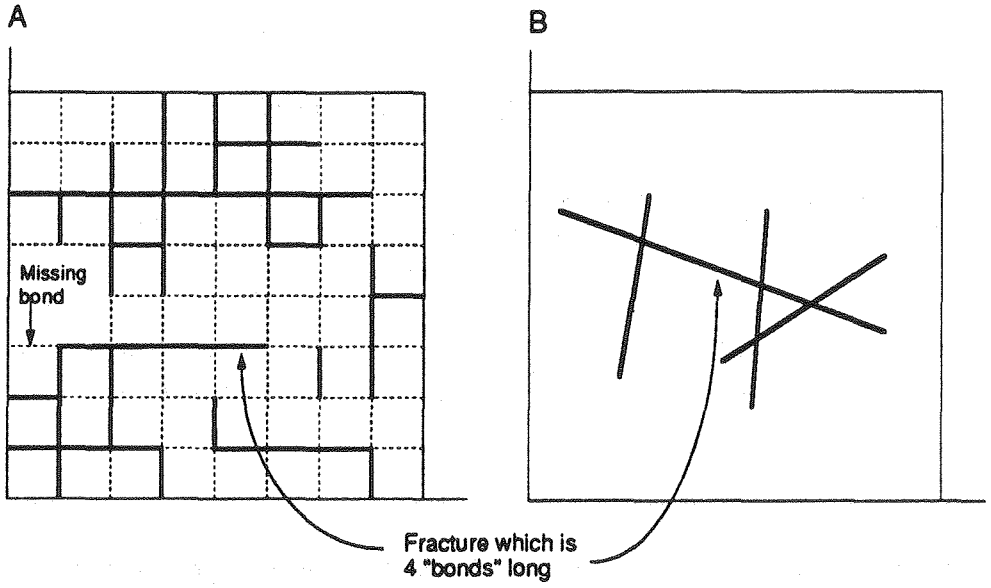

Figure 2.3. Correspondence of "average run length" between the regular lattice model and the Poisson model.

The resulting average line length in units of bonds is

$$\sum_{k=1}^{\infty} k(1-p)^2 p^{k-1} k = \frac{1+p}{1-p} .$$

Now consider an arbitrary line in the random line system. One can view that line as being made up of bonds, each bond being a piece of the line between two intersections, Figure 2.3b. The average length of a line in units of bonds is then the average number of intersections per line plus 1, that is $\zeta + 1$.

Equating the two average lengths described above gives

$$\zeta + 1 = \frac{1+p}{1-p}$$

or

$$p = p(\zeta) = \frac{\zeta}{\zeta+2} . \tag{2.7}$$

This expression for $p(\zeta)$ yields the following expression for permeability based on percolation theory (equation 2.1):

$$\frac{K}{K_S} = \kappa \left[\frac{\zeta}{\zeta+2} - \frac{\zeta_{crit}}{\zeta_{crit}+2} \right]^t \tag{2.8}$$

where κ is a constant.

In order to use $p(\zeta)$ in equation (2.3) for equivalent media theory it is necessary to calculate a modified coordination number $z(\zeta)$, for a random line system. The coordination number of a regular lattice is the number of bonds connected from a site. In the rectangular lattice in Figure 2.1a-d the coordination number is $z = 4$. In a random line system (Figure 2.1e-h) we propose an average coordination number:

$$z = z(\zeta) = 4\left(1 - \frac{1}{\zeta}\right) . \tag{2.9}$$

The reason for a coordination number smaller than $z = 4$ is shown in Figure 2.4. Here we can see that the two fracture intersections on the ends of a typical line only have coordination number $z = 3$; the ends of the line do not count because they will never contribute to flow. The sites in the center of a line segment will have coordination number $z = 4$. In fact, the sites on the end of a line can have coordination number $z = 2$ if that site is also on the end of the other intersecting line as shown in Figure 2.4. For the same reason sites in the center of a line could have coordination number 3. The average fraction of center sites is $(\zeta-2)/\zeta$ and the fraction of end sites is $2/\zeta$. Hence a site on the end of a line will have average coordination number:

$$3\cdot\left(\frac{\zeta-2}{\zeta}\right) + 2\cdot\frac{2}{\zeta} = 3 - \frac{2}{\zeta} .$$

Similar reasoning gives an average coordination number of

$$4\cdot\left(\frac{\zeta-2}{\zeta}\right) + 3\cdot\frac{2}{\zeta} = 4 - \frac{2}{\zeta}$$

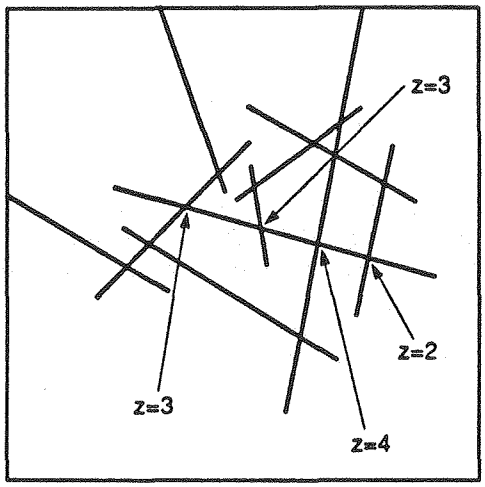

XBL 8812-8648

Figure 2.4. Coordination numbers in a Poisson model.

for a site in the center of a line. Finally, because the average fraction of center sites is $(\zeta-2)/\zeta$ and the average fraction of end sites is $2/\zeta$, we obtain an overall average coordination number of

$$z(\zeta) = (\frac{\zeta-2}{\zeta}) \cdot (4-\frac{2}{\zeta}) + \frac{2}{\zeta} \cdot (3-\frac{2}{\zeta}) = 4(1-\frac{1}{\zeta})$$

This modified coordination number, given by equation (2.9), coupled with $p(\zeta)$ in equation (2.7) then yields:

$$\frac{K}{K_S} = 1 - \frac{z(\zeta)(1-p(\zeta))}{z(\zeta)-2} = \frac{\zeta(\zeta-4)}{(\zeta^2-4)} \qquad (2.10)$$

Figure 2.5a shows a plot of ζ vs K/K_S derived from our parameter studies for cases above the critical limit. Each point on the plot is an average permeability measured as close as possible to the scale of the REV from a realization of a random line system (Hestir and Long, 1989). The dotted curves are calculated from the theoretical relationship between ζ and average permeability from equivalent media theory (Equation 2.10). The dashed curves are from percolation theory (Equation 2.8) with a fitted value of κ=4.01. Figure 2.5b and 2.5c show the same information plotted as a function of p. The curves in Figures 2.5b and 2.5c have the classic shape seen in the literature.

Details of the parameter settings used for each point are given in Hestir and Long (1989). In each case a different seed was chosen for the pseudo-random number generator used to create the realization. The parameter values for the different cases were chosen to illustrate the fact that ζ can be used to predict permeability for a wide variety of random line systems. We briefly describe these below.

To begin with, eight cases were chosen with approximately the same value of $\lambda_l = 0.576$ and the same orientation distribution. The orientation distribution is a mixture of two normals, one with an average of 0° and an standard deviation of 20°, and the other with an average of 90° and a standard deviation of 20°. This orientation distribution is equivalent to generating two sets of fractures where each set is assumed to have the same areal density and constant length. A numerical calculation gives $H(\Theta) = 0.62$ in this case. Each case has the same value of λ_l, but different values of λ_A and l such that $\lambda_l = \lambda_A \cdot l$.

Four cases have the same area rate, λ_A, and constant line lengths, l, but the standard deviation of the orientation distributions is varied. Each of these cases has a normal orientation distribution with different

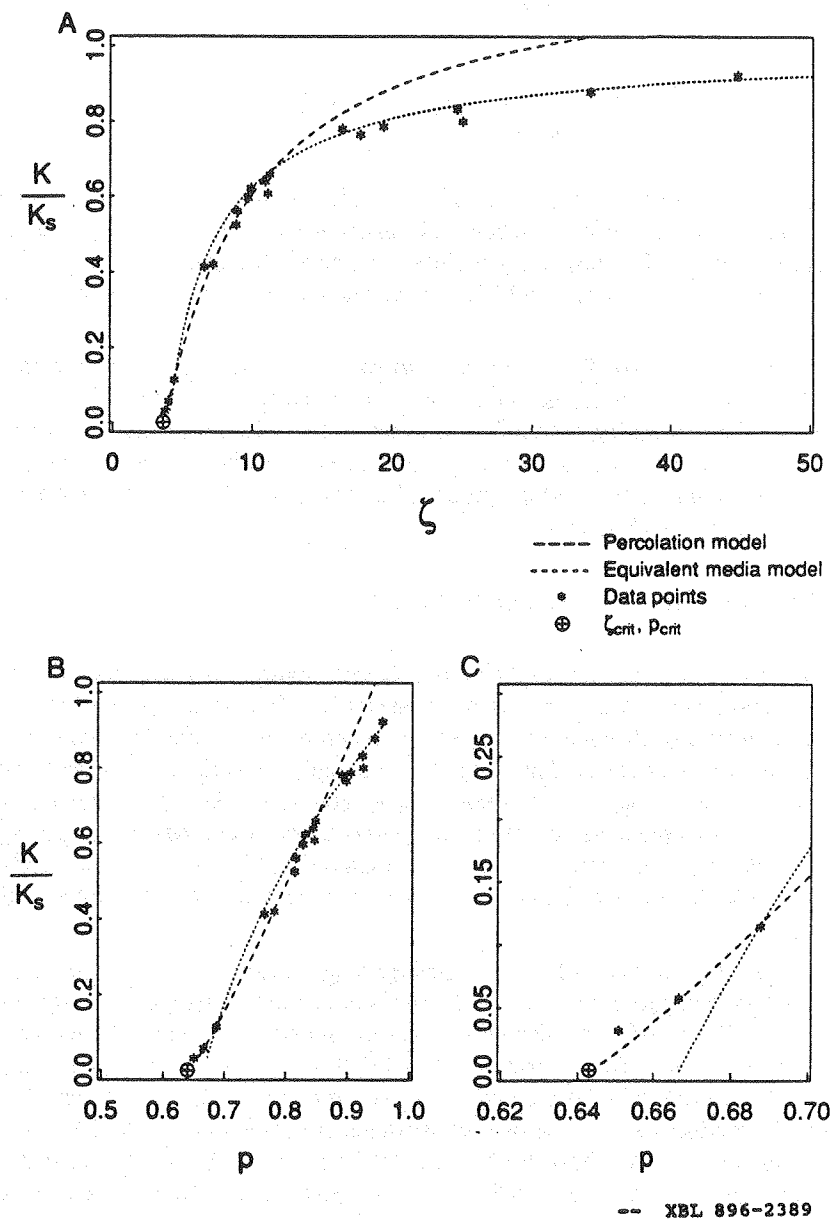

Figure 2.5. a) Results of the parameter studies plotted against ζ, b) and c) plotted against p.

standard deviations which has the effect of changing $H(\Theta)$ and hence ζ. This tests the effect of the orientation correction factor $H(\Theta)$.

Four cases have the same normal orientation distribution with a standard deviation of 70° yielding $H(\Theta) = 0.58$. They have a value of λ_t approximately equal to 0.288 which is about half that of the other cases. This tests the effect of using a different λ_t which is equivalent to changing K_S.

Three cases are included which are near the critical limit and these are shown most clearly in Figure 2.4c. Each of these cases has a uniform orientation distribution which gives $H(\Theta) = 2/\pi$. In addition to this data, a percolation frequency study of near critical Poisson graphs indicated that percolation frequency was 50% when ζ equals 3.6. By fitting all this data to Equation 2.8, we obtain a value of $\zeta_{crit} = 3.6$,

κ=4.01, p_c=0.64 and the exponent t = 1.1 which conforms to values found in percolation literature. In other words:

$$\frac{K}{K_S} = 4.01\left(\frac{\zeta}{\zeta+2} - .64\right)^{1.1} \qquad \text{for } \zeta \geq 3.6$$

One other set of cases for variable fracture length is included in this figure. Four cases have lognormal distributions for length with different coefficients of variation (ratio of standard deviation to mean). One has an exponential distribution for length. Each of these cases has the same orientation distribution as that used in the first eight cases. The way in which ζ is calculated for these cases is a special case discussed below.

Figure 2.5 shows that on the whole, we are able to calculate permeability well with our model. From Figure 2.5a and 2.5b we see that for all values of ζ significantly greater than ζ_{crit}, the data fit the equivalent media model. The percolation model fits much better for values near ζ_{crit} up to values of ζ of near ten or twelve. One anomalous value is for the smallest value of ζ shown. In this case, the value of permeability measured is too high for either of the models, but this is most likely due to the fact that it was not possible to measure a large enough sample.

2.5. GENERAL EXTENSION TO THE VARIABLE LENGTH CASE

The reason that variable length systems are a special case is that studies have shown that eliminating the shortest fractures up to some cutoff value, c, has no measurable effect on the permeability (Hestir and Long, 1989). However, eliminating all fractures shorter than a cutoff c will increase $\bar{l}$ and decrease λ_A and thus will change the value of ζ. This means that we could have many networks with the same permeability but different connectivities which would imply a non-unique relationship between connectivity and permeability. In order to avoid this problem, we define the connectivity of the variable length system to be the ζ for the system with the maximum truncation of short fractures that still has the same permeability as the original network. We use this value of ζ to extend the above percolation and equivalent media models to random line systems.

Figure 2.6 illustrates the definition of ζ for a random length system. Data for this plot is derived from a fracture network with a negative exponential distribution of fracture lengths. In Figure 2.6a, K and ζ are plotted as functions of the cutoff c. We define the connectivity of the system to be the value of $\zeta(c_0)$, marked by the dashed vertical line. This is exactly the point at which $K(c)$ starts to decrease. The networks corresponding to the untruncated system and the system truncated at c_0 are shown in Figures 2.6b and 2.6d. The respective conducting portions of these systems are shown in Figure 2.6c and 2.6e where dead ends and non-conducting elements have been removed. One can see by inspection that the reduced networks (2.6c and 2.6e) are nearly the same which explains why the small fractures have a negligible effect on permeability.

To find an expression for $\zeta(c)$ we first find expressions for fracture density and average length as functions of c. To calculate the fracture density, we need a correction factor $G(c)$ such that after truncation at c the density will be $\lambda_A G(c)$:

$$G(c) = \int_c^\infty f(l)dl = 1 - \int_0^c f(l)dl$$

Similarly, to find the average length, we calculate the correction factor $F(c)$:

$$F(c) = \int_c^\infty lf(l)dl = \bar{l} - \int_0^c lf(l)dl \ .$$

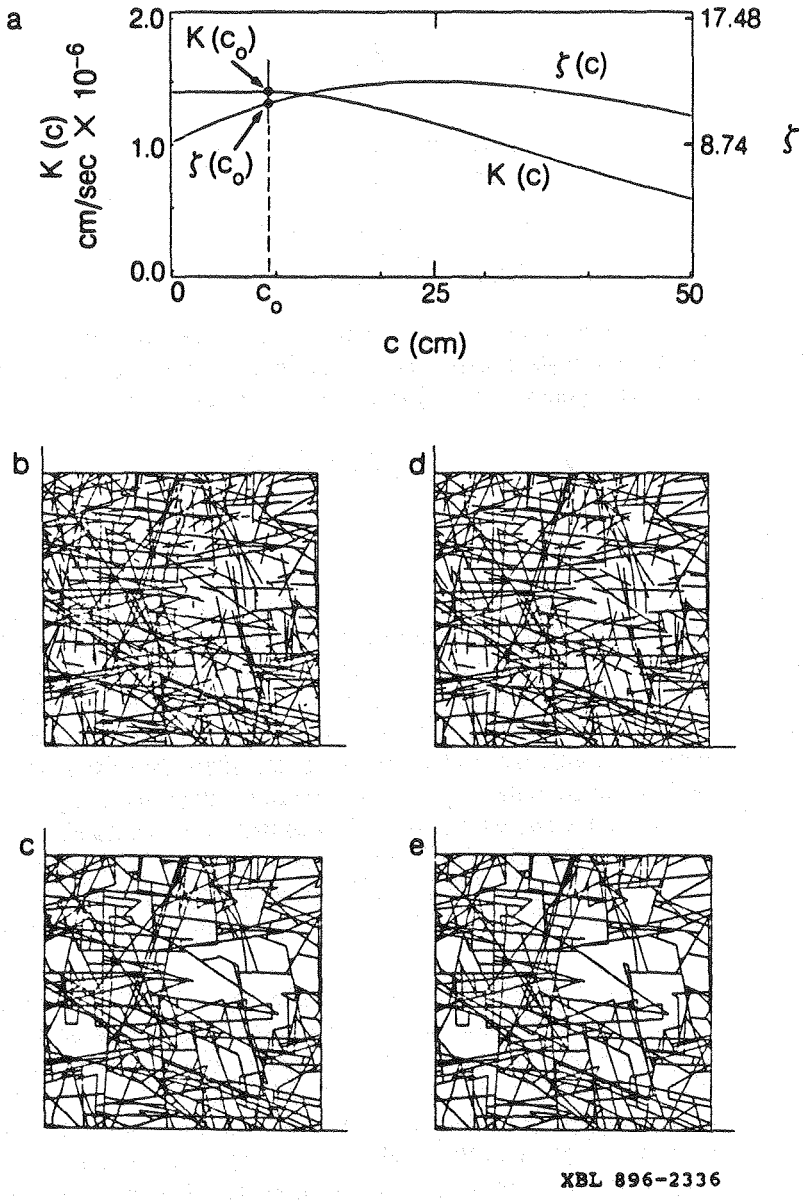

Figure 2.6. a) Definition ζ for a random length system, b) untruncated network, c) conductive part of (b), d) system truncated at C_0, e) conductive part of (d).

This gives average line length after truncation at c to be

$$\frac{F(c)}{G(c)}.$$

Substituting into Equation 2.6, truncation at c will yield a new value for ζ given by

$$\zeta(c) = G(c)\lambda_A \frac{F^2(c)}{G^2(c)} H(\Theta) = \lambda_A \frac{F^2(c)}{G(c)} H(\Theta) \tag{2.11}$$

and a new value of Snow's permeability:

$$K_S(c) = k_0\lambda_l = k_0\lambda_A\bar{l} = k_0\frac{F(c)}{G(c)}G(c)\lambda_A = k_0F(c)\lambda_A \tag{2.12}$$

where k_0 is a constant determined by the units and the conductance of the fracture elements. Taking $c = c_0$ and substituting this into Equation 2.11, we have the model based on Equation 2.10

$$\frac{K(c_0)}{K_S(c_0)} = \frac{\zeta(c_0)(\zeta(c_0)-4)}{\zeta^2(c_0)-4} \tag{2.13}$$

where $K(c_0)$ is the permeability of both the untruncated and the truncated system and $K_s(c_0)$ is given by Equation 2.12. In order to find an analytical expression for c_0 in terms of ζ, Hestir and Long (1989) show that c_0 is the root of a fourth degree polynomial in ζ which corresponds to maximizing $K(c)$ in

$$K(c) = k_oF(c)\lambda_A\frac{\zeta(c)(\zeta(c)-4)}{\zeta^2(c)-4}$$

2.6. CONCLUSIONS

Above we have summarized work which allows one to calculate the value of permeability for a two-dimensional Poisson fracture system where the fractures all have the same conductance. The model works for any distribution of fracture length, density and orientation. It remains to extend the model to the case of variable fracture conductance. Variable conductance can also be thought of as a kind of connectivity in that fractures with small values of conductance form bottle necks and thus decrease the degree of connection. This is a problem that was partially solved by Charlaix et al. (1986) for constant length fractures. In this case, one can order the fractures from the largest to the smallest conductance. By placing the fractures in the network from the smallest to the largest, Charlaix showed that the conductance of the fracture at the critical limit of connectivity controls the conductance of the network. However, the case of variable length combined with variable conductance is more complicated because the high conductivity fractures may be short and thus not contribute much to the connectivity. This problem has not to our knowledge been solved.

Work such as this shows that if we know the conceptual model which describes a fracture network and the parameters of the statistical distributions which govern the connectivity of the network, we can know the connectivity and therefore something about the hydrologic behavior. For this reason it is attractive to make measurements of fracture geometry in the field and from this data try to build a model of a fracture network. The Poisson model is probably not a good basis for the conceptual model because it is too simple. Fractures often occur in related clusters and this violates the rules of a simple Poisson process. In the next section we briefly review work done to predict hydrologic behavior from a geometric analysis of the fracture pattern where we have used a complex Poisson model called the Parent-Daughter model.

3. Field Experience

The theoretical work described above shows how fracture geometry statistics can be used to understand the hydraulic behavior of a network of fractures. If statistics describing the geometry of a real fracture network can be specified, we have good reason to believe that the hydrology of this network can be understood. Below, we describe the types of data that can be obtained and summarize our experience with using this geometric information to build a model of a real fracture network.

The fundamental problem in modeling fracture hydrology is that the medium does not behave as a continuum. Parts of the rock have no hydraulic communication with other parts. In the case where the matrix rock can be considered impermeable, this fundamental behavior is governed by the geometry of the fracture network. If a connected cluster of conductive fractures links point A and point B, there can be

flow between the two points. If not, then there is no flow. This heterogeneous connectivity is very commonly observed in fractured rock. As a consequence of this observation, attempts at building a fracture hydrology model should be focussed on reproducing, a least in a statistical sense, the geometry of the fracture network. This involves determining a statistical rule for locating fractures, determining their orientation, size and conductivity. Then the interconnections between the fractures can be found and flow patterns calculated.

Data available for fracture hydrology models might include:

1. Fracture trace maps from drift walls or surface exposures giving fracture location, orientation, trace length, coatings, roughness etc.
2. Fracture logs from boreholes giving fracture location, orientation, coatings, roughness etc.
3. Bore-hole geophysical logs
4. Single-hole packer tests
5. Cross-hole and reflection geophysics
6. Cross-hole hydraulic tests

An interpretation was made of the data at the Fanay-Augères mine in France (Billaux et al., 1989) using data which included samples from numbers 1, 2 and 4 above. The analysis was based on assuming the fractures were disc-shaped and uniformly permeable in their plane. In order to represent the clustering of fractures, the arrangement of fractures in space was a complex Poisson process called the Parent-Daughter process. Geostatistical techniques were used to fit the parameters of the model based on data on trace lengths, orientation and fracture frequency. A pattern of fractures in a 100m cube was determined.

Conclusions from this effort were very striking. First we found that the use of one- and two-dimensional data to infer three-dimensional geometry is an impossible task. Many three-dimensional geometries can account for the same one- and two-dimensional data. Second, no matter how the three-dimensional geometry was determined, there were far too many fractures to account for the lack of connectivity known to exist. Figure 3.1 shows the fractures greater than one meter in diameter that were predicted to intersect a 2.5m sphere for two parts of the drift, S1 and S2. If all the fractures were present and hydrologically active the medium would have behaved like an equivalent continuum. However, cross-hole hydrologic and tracer test results showed that this was definitely not the case.

In order to make this geometric approach successful we need somehow to constrain the three-dimensional geometry and more importantly we need to find some way to account for the parts of the fracture system which do not conduct water. We suspect that many cases are similar to Fanay-Augéres in that the fractures are relatively pervasive and the real problem is finding what parts of the system actually conduct.

Fanay-Augères offered one other key fact in this regard. The two drifts were mapped in this mine: one wet (S1), one dry (S2). For both drifts the fracture geometry seemed to indicate highly connected fracture networks. However, in the wet drift, a major fault ran through the block of rock surrounding this portion of the drift. It seems that the hydrology of the site is controlled by major features i.e. fracture zones. This observation is certainly not confined to Fanay-Augères. Investigations at the Stripa Mine in Sweden reported on by Olsson et al. (1988a) found that 94% of the hydraulic transmissivity is found in 4% of the tested rock. Similar conditions exist at many other sites. This provides strong evidence for the role of fracture zones in controlling the hydrology. Further, cross-hole hydraulic responses are often very non-uniform. For example, at the Stripa mine, geophysics have indicated that a disproportionate number of fracture zones intersect a particular borehole called W2. While this borehole was being drilled, the observed heads in the entire vicinity dropped significantly and a similar response is observed each time W2 is opened or closed whereas the drilling or opening of other holes had little effect (Carlsten et al., 1988). Another example comes from Hsieh et al (1985) who performed cross-hole hydraulic tests in a ubiquitously fractured granite but found that certain zones had no hydraulic connection to others. It is possible to find many other references which describe the same phenomena. From these facts we infer that the

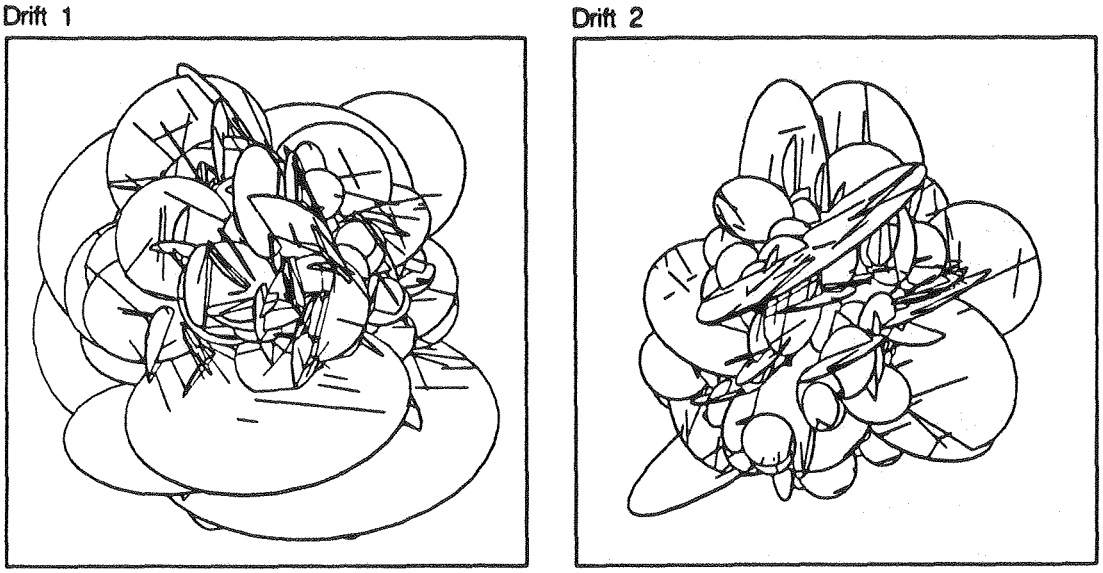

Figure 3.1. Fractures greater than 1m in diameter predicted to intersect a 2.5m sphere for a) S1, and b) S2 at Fanay Augéres.

hydrology of many fractured sites is controlled by a finite number of major conductors that form a three-dimensional network of unknown configuration. It is often likely that a few major features dominate the entire hydrology of a given site.

3.1. CONCLUSIONS

Our experience so far has indicated that focussing on the details of fracture geometry statistics is equivalent to "not seeing the forest for the trees". If fracture zones control the hydrology, then efforts should first be aimed directly at locating and characterizing fracture zones. Further, one should concentrate on determining the hydrologic characteristics of the zones. We expect that zones are not continuous and that the permeability structure within the zones is complex. Therefore, we propose a different approach for building a fracture hydrology model. This approach concentrates on identifying the location of zones and the nature of permeability within the zones. To obtain a model of the first order hydrologic behavior, we model only the major hydrologic features. We assume that these features are associated with the fracture zones. A fracture zone is then assumed to be consisted of a two-dimensional network of hydrologic conductors.

For location of the zones, we rely heavily on the recent advances in geophysics that have allowed fractures zones to be "seen" inside the rock. Then, based on these we build a hydrologic conceptual model of the the rock which we call a template. The template should contain all the likely major conductors and is the basis for fluid flow calculation. We infer as much as possible about the qualitative hydrologic attributes of the zones through geology and geomechanics. Finally, we throw away conductors in a manner that conditions the model to observed well test behavior. In other words, within the template we identify patterns of conductance that can explain the observed hydraulic behavior. We do this in two ways. First, we identify the fractal dimension of flow using Barker's (1988) analysis and relate this to the connectivity, and the connectivity to the percentage of conductances present in the template. Second, we use simulated annealing to arrange the conductances such that they explain observed distributions of head, observed fluxes, or observed tracer test results.

This model building approach that is currently being applied to data from Stripa and another data set from the Grimsel Rock Laboratory in Switzerland. The experience at Stripa will be summarized below and is given in detail in Long et al. (1989).

4. Fracture Flow Modeling at Stripa

Investigations related to the geologic storage of nuclear waste have been ongoing at the Stripa Mine in Sweden for more than ten years. The latest of these investigations is called Phase III and is sponsored by OECD Nuclear Energy Association (NEA) as an international cooperative effort managed by the Swedish Nuclear Fuel and Waste Management Company (SKB).

The Stripa Phase III project includes the Site Characterization and Validation (SCV) experiment, which is designed to test current abilities to characterize fractured rock before it is used for nuclear waste storage. The effort is centered on a block of rock 150 x 100 x 50 m in size at a depth of about 330m. The block lies between previous experimental sites, the Macro-permeability/ Buffer Mass Test site and the 3-D Migration site (Figure 4.1). One aim of the SCV work is to predict the inflow into a drift, called the "Validation Drift" before the drift is excavated and the inflow is actually measured. We present a preliminary prediction below.

The Validation Drift has not yet been excavated, but the prediction of inflow described here can be compared to a measurement that has been made of inflow into five pilot boreholes which have been drilled

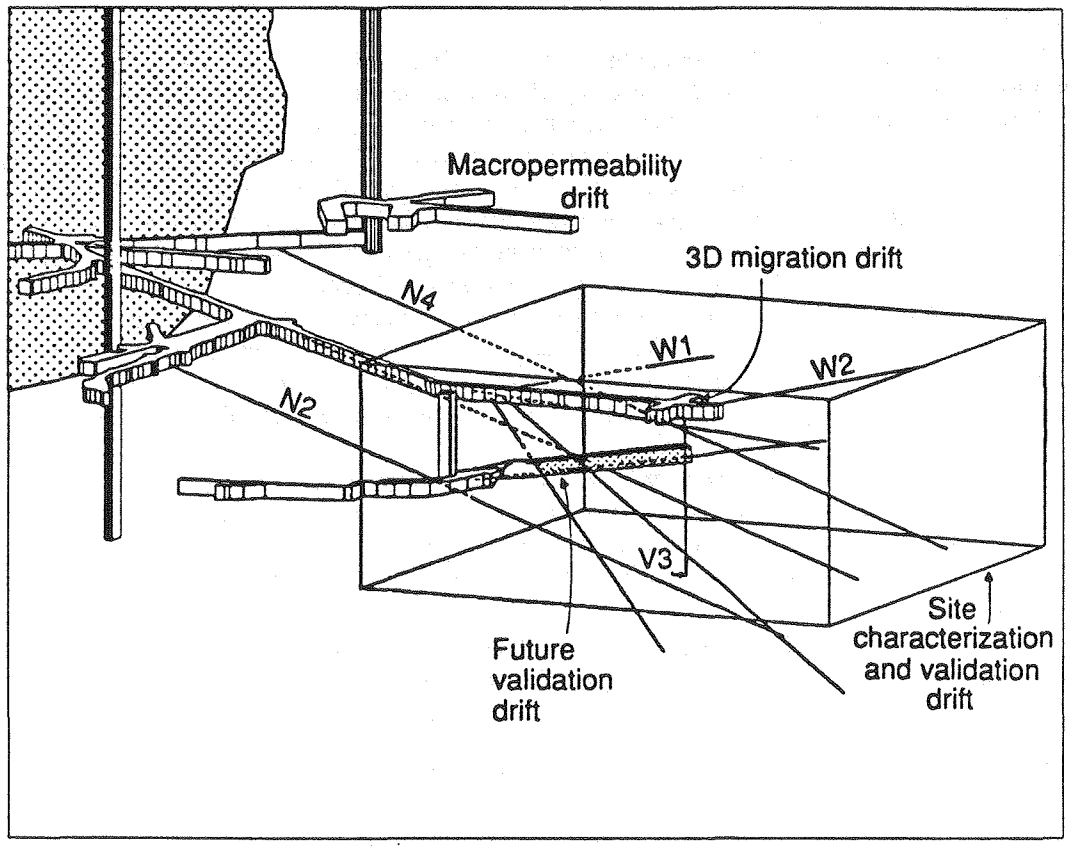

Figure 4.1. Perspective view of the SCV block. Dotted area in the upper left is the mined out stopes (after Olsson, 1988a).

along the periphery plus one in the center of the future drift (the D-holes). As our prediction does not account for the effects of excavation (such as stress effects or the effect of an air-interface at the drift wall), the comparison of our prediction with the borehole inflow is in some ways better than the comparison with the actual inflow to the drift.

The prediction is based on data from a series of boreholes drilled throughout the block. Data from six boreholes (N2, N3, N4, W1, W2, and V3) include fracture characteristics, stress, single borehole geophysical logging, cross-hole and reflection radar and seismic, and single hole packer test measurements. Maps of fracture traces on the drift walls have also been made. Olsson et al. (1988a) gives background information describing the site and the results of the borehole investigations. Cross-hole hydrologic tests are planned in the near future.

The interpretation of seismic and radar tomography data has predicted six major fracture zones. We have compared the zones with the single hole hydrologic tests to see if the geophysical zones could account for the hydrologic anomalies. Based on these studies we developed a hydrologic conceptual model where all the conductive elements of the model are confined to fracture zones. Based on examination of the boreholes and drift walls, we have modeled the zones as planes with a square grid of conductors that form the possible paths for fluid flow.

In order to determine which of the grid elements are active and which are inactive, we can employ two techniques. First, a technique is under development for determining the percentage of grid elements likely to be present based on cross-hole well test response. In this technique we assume that the connectivity of the grid elements is reflected in the well test behavior as a fractal dimension. Thus given the fractal dimension from a well test response, we could determine the percentage, p, of grid elements that would give the same fractal dimension. This technique has not yet been applied to the Stripa data, but it is described in Long et al. (1989).

A second technique is called "Simulated Annealing". Simulated annealing is an inverse technique which is used to find the pattern of conductances which cause the model to behave in the way the the insitu tests behaved. First, well tests that were performed insitu are numerically simulated in the model using the network generator, CHANGE plus the fracture flow code, TRINET (Karasaki, 1988). Then the "Simulated Annealing" algorithm is used to modify the model until the behavior of the model matches the observed behavior. This is done by randomly eliminating or restoring a conducting grid element and recalculating the response to the well test with TRINET. We compare the behavior of the new model to the old and decide whether or not to keep the change. This process is repeated many times until the model matches the observed behavior. The algorithm is designed to find an arrangement of conductors that responds to the well test in nearly the same way that the real well test was observed to respond. This final configuration of the grid can be considered as an averaged, "rastorized" version of a possible conductance geometry. Finally, the boundary conditions imposed on the model can be changed in order to make predictions of flow that have not been measured.

At the current stage of the project, there are no cross-hole hydrologic data available on which to base the annealing. As a result a preliminary analysis was made by developing a synthetic cross-hole test based on various sources of information. The results are preliminary, but the exercise provides a good description of the methods. At a later date we will use the actual cross-hole tests to re-calculate inflow into the D-holes.

Below we review the data and the development of the conceptual model. Then we explain the theory behind annealing and the construction of the synthetic cross-hole test. Finally we give the results of the modeling effort and show how they compare to the actual analysis.

4.1. IDENTIFICATION OF FRACTURE ZONES WITH GEOPHYSICS

An extensive geophysical data set has been collected in the SCV block at Stripa in order to locate and characterize fracture zones. These are described in Olsson et al. (1988b). Both radar and seismic methods were used. For both techniques cross-hole tomographic and reflection data was collected.

Seismic signals are sensitive to changes in rock density, porosity, and water content as well as fracture stiffness and orientation. Both slowness and attenuation tomograms can be produced, but attenuation tomograms are often unreliable due to poor source and receiver coupling and non-repeatability of the source. Radar signals are sensitive to changes in dielectric constant and electrical conductivity (Sen et al., 1981). Both the electrical conductivity and dielectric constant increase with the water content. The radar slowness tomograms depend only on contrasts in dielectric constant and attenuation depends on the ratio of the dielectric constant to the conductivity. As there is more contrast between values of electrical conductivity than between values of dielectric constant, the attenuation tomograms are subject to fewer errors and the image is more clear. In granitic rock, it is assumed that most rock matrix properties are relatively constant so that hydrologic features such as fracture zones and increased porosity and water content will show up as the anomalies. For this reason the geophysics allows us to "see" into the rock and predict where the major fluid conductors are. However, rock properties are not always constant and sometimes the identified anomalies have little to do with hydrology.

An example tomogram from the Stripa site is shown in Figure 4.2. An integrated analysis of these tomograms plus all the other geophysical data was used to make an interpretation of the location and extent of major features in the block. This resulted in the identification of five major fracture zones called A, B, C, Ha, Hb and I. Zones A, B, C, strike approximately North-East and dip about 45 degrees to the South-East. The Ha, Hb, and I zones are nearly vertical and strike North-South (Figure 4.3). A further feature, called Q was identified as a circular feature just south of the B zone at the west end of the block.

4.2. THE HYDROLOGIC CONCEPTUAL MODEL

Figure 4.3 (after Olsson et al., 1988a) gives an example from hole N2 of the summary of the borehole data acquired for the N- and W-holes. Hydrologic zones are marked in the right hand column. The geophysical features are shown on the plots as horizontal bands. Under the hydraulic conductivity column, we have blackened in those conductivities greater than 10^{-8} m/s. Ten meters is a reasonable width for a fracture zone in rock at Stripa. If the geophysical features are taken to have a hydraulic width of about ten meters, they account for about 60% of the measured hydraulic transmissivity measured in the boreholes. Almost all of the remaining 40% of the transmissivity is accounted for in three zones: at 80 meters in borehole W2, 152 meters in N2 (see Figure 4.3) and from 80 to 90 meters borehole N4. By revisiting the original geophysical data we can see that there are strong radar and seismic anomalies at each of these zones. These anomalies were excluded in the process of making the geophysical interpretation because they are not substantiated in all the data. For example, Figure 4.4 shows another radar tomogram which has a strong anomaly near 100m in borehole N4. This anomaly is not present in Figure 4.2.

The simplest way to account for the remaining hydrologic anomalies in N4 and N2 was to add another zone, B'. Figure 4.5 shows a perspective plot where zones B and C are represented as dots located on planes. In this figure we are looking along the B and C planes so that the zones appear as dots clustered along a line. In this perspective, one can see that the hydrologic anomalies in N4 and N2 lie on a plane roughly half way between zone B and zone C. For this reason, we chose B' to be a plane between B and C and parallel to the A, B, and C zones. The addition of B' increases the percentage of transmissivity accounted for to about 78%.

The new zone intersects the hole N3, but there is no similar hydrologic anomaly in N3 at this point. The fact that a zone is not uniformly conductive is not a problem for this model. This can easily be accounted for if no permeable channel from B' intersects N3. We are more concerned with insuring that channels are possible where hydrology has been observed. Extra channels can always be made inactive in the annealing process described below.

The B' zone also fits in well with the geophysical results. The radar results show a very strong low velocity zone in the section N4-N3 slowness tomograms corresponding to the feature at 90 meters down borehole N4 (Figure 4.4, from Olsson et al., 1988b) as well as single hole radar reflectors on either side (Olsson et al., 1988b).

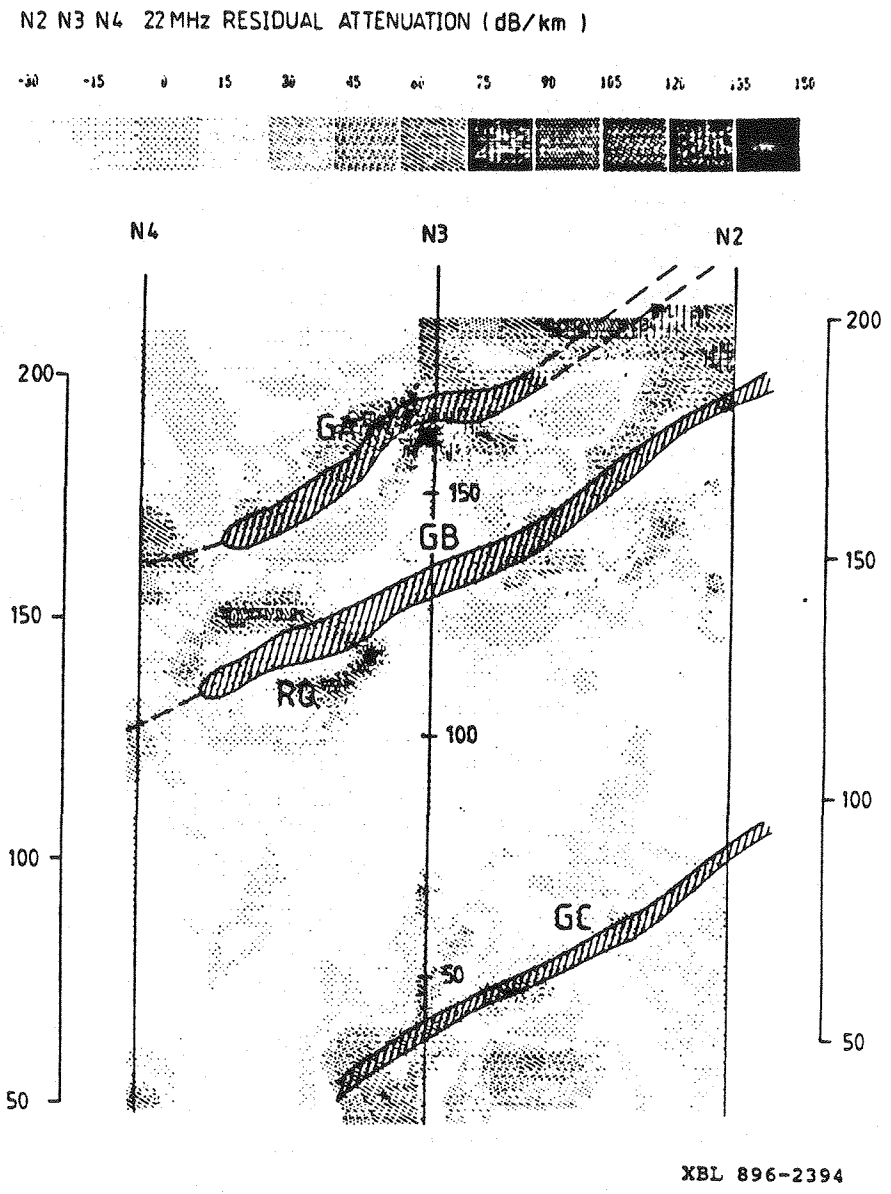

Figure 4.2. Example radar attenuation tomogram between holes N4 and N2 showing predicted fracture zones A, B and C (Olsson, 1988a).

The B' feature may be related to the RQ feature shown on Figure 4.2. This tomogram shows the B' (or RB) anomaly begins to peter out about 20 meters from the borehole. It appears that it may intersect the South edge of the RQ feature. The feature B then skirts the North edge of RQ and produces the largest hydrologic anomaly in N3. It may be that RQ is a step between *en echelon* fracture zones represented by B' and B. This would also explain the lack of hydrologic activity in N3 at B'. However, it does not explain why B' is again the largest anomaly in N2 unless there is another step in the opposite direction.

One remaining anomaly in W2 between zones H and B (called HB* in Table 4.1) accounts for 21.7% of the transmissivity. If we allocate this transmissivity partly to H and partly to B, then we have accounted for 98.7% of the observed transmissivity with a zone model. This makes a certain amount of sense when we consider that the transmissivity measured in the boreholes is not strictly additive because

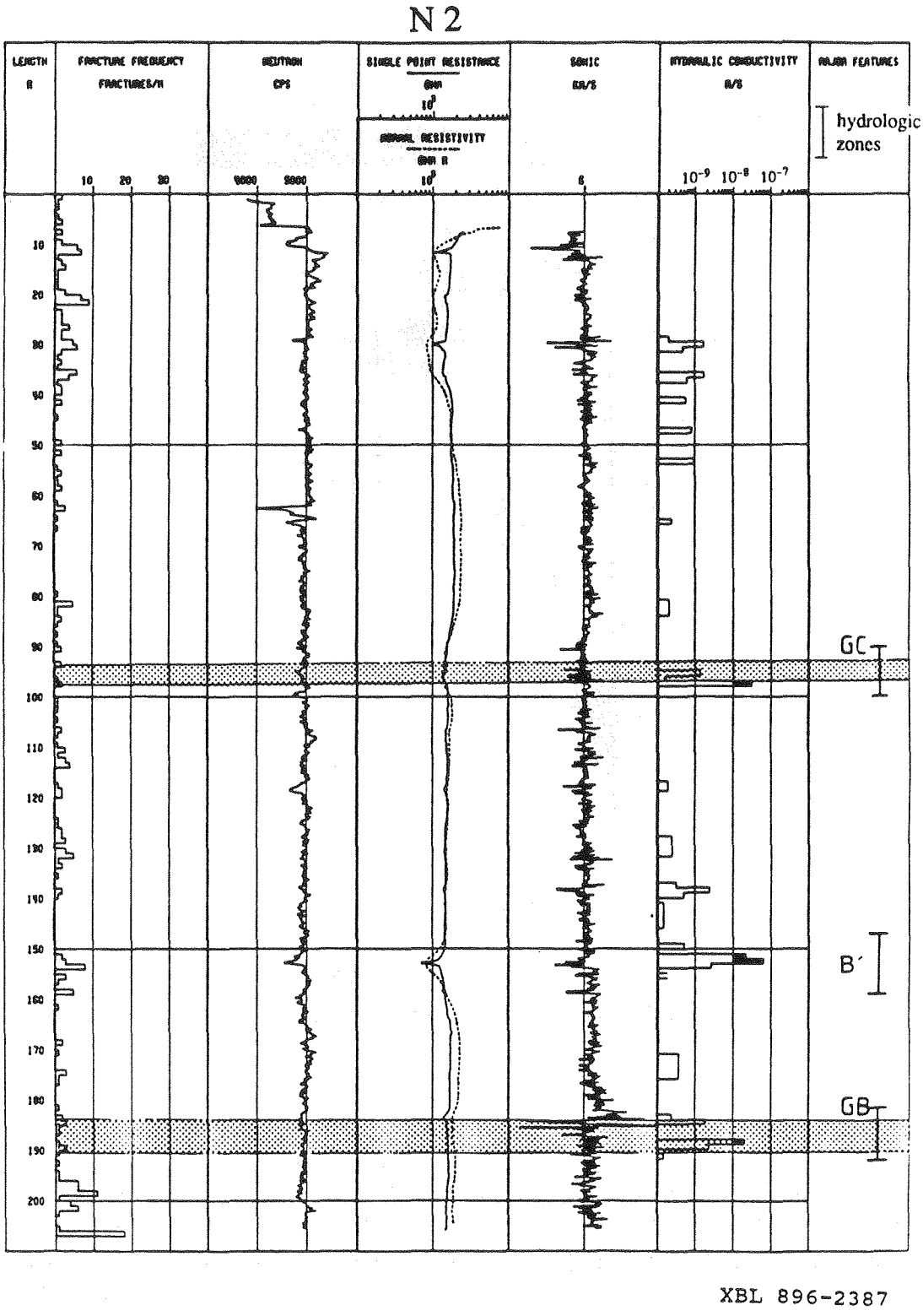

Figure 4.3. Summary data sheet for N2. Hydraulic conductivities greater than 10^{-8} m/s have been blackened in. Hydrologic zones are marked in the right hand column (after Olsson, 1988a).

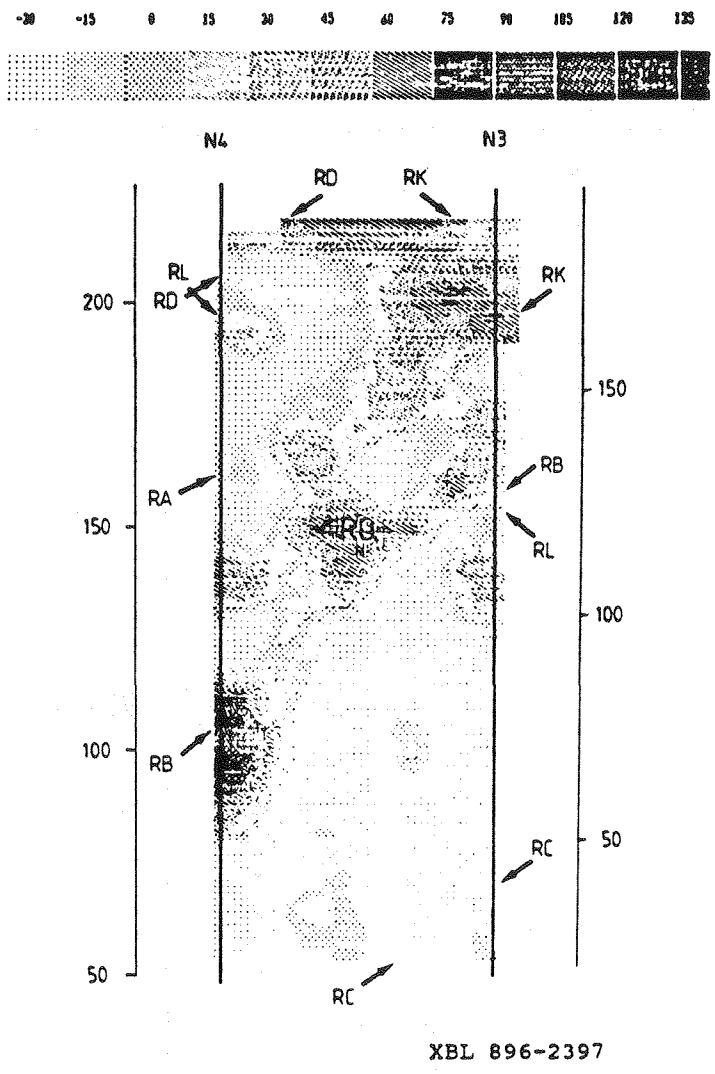

Figure 4.4. Example residual radar slowness tomogram for the borehole section N3-N4 made with a center frequency of 22 MHz (Olsson, 1988a).

successive borehole tests are actually sampling some of the same transmissivity. It is easy to imagine that the high conductivity found between zones H and B in W2 is due to a few conductive features that are related to H and B and possibly related to the intersection of H and B.

The resulting hydrologic zone model is shown in Figure 4.6 in a perspective view from the North-West. Zones A, B, B', C, Ha, Hb and I are shown. Gridding on the planes represents the hydraulic conductors of the template used for annealing. The zones are disc-shaped planes. As we do not expect the zones to be uniformly permeable, the zones are discretized into flow channels within the region of interest. Any type of discretization could be used. The choice of grid is made with the support of geomechanical investigations of the shear zones explained below.

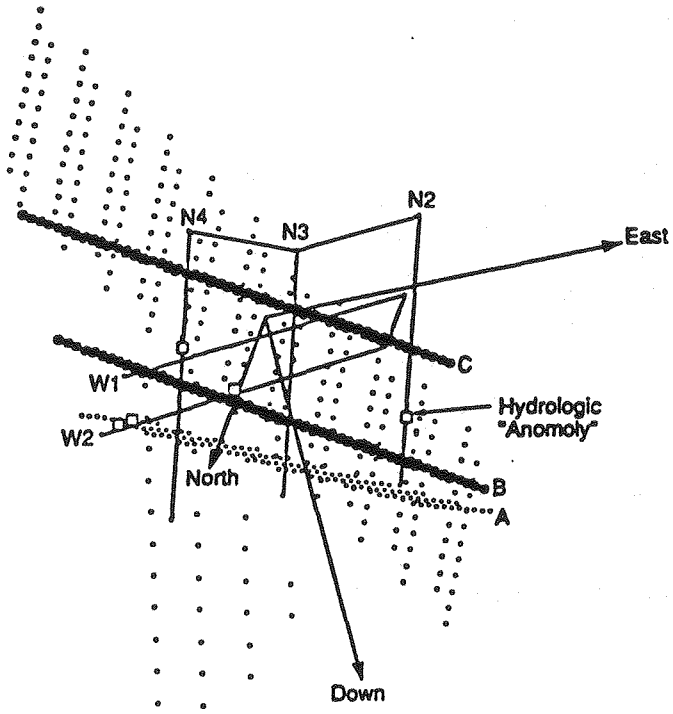

Figure 4.5. A perspective view of the SCV block looking up to the North-East showing zones B and C and that two hydrologic anomalies lie between these zones in the plane parallel to them.

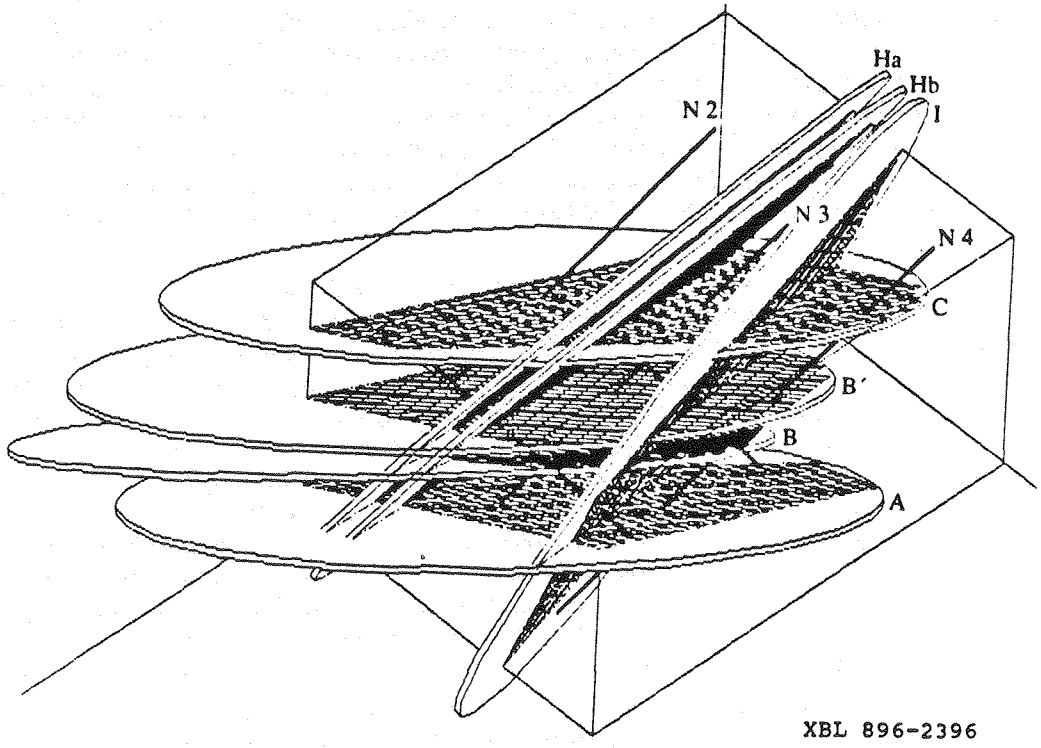

Figure 4.6. The hydrologic zone model shown in perspective from the North-West looking down. Zones A, B, B', C, Ha, Hb and I are shown. Gridding on the planes represents the hydraulic conductors of the template used for annealing.

Table 4.1. Hydraulic Transmissivity Distribution

Hydraulic Transmissivity (10^{-9} m^2/s)							
Zone	W1	W2	N2	N3	N4	Total	% of total
A	-	99	-	0	1	100	3.2
B	0	88	20	12	5	125	4.0
B'	-	-	80	0	450	530	17.1
C	-	-	36	0	0	36	1.1
H	120	950	-	-	-	1070	34.5
I	25	510	-	-	-	535	17.2
(HB*)	-	670	-	-	-	670	21.6
Sum						145	2317
Total transmissivity						3100	100

* Transmissivity between zones H and B in borehole W2

4.3. GEOMECHANICAL INTERPRETATION OF THE SHEAR ZONES

We have evidence that the major zones are fault zones under reverse dip-slip motion. Associated with slip in the zones, secondary fracturing has been observed. For the NE-striking, low dipping zones (A,B, B',C), the secondary fractures are sub-horizontal, and for the N-S striking, steeply dipping zones (Ha, Hb, I), the secondary fractures strike N-S and dip 10-40° to the east. Numerical modeling indicates that under the present stress state in the SCV block, the sub-horizontal secondary fractures could be open and have a much higher conductivity than other fractures in the SCV block. This, along with the higher fracture densities in the zones, may explain why the conductivity in the zones is greater than the surrounding ground. Also, this will cause anisotropy in flow in the zones, with preferred pathways in the direction of the secondary fractures. Though not discussed in this paper, there is evidence that zone intersections may be important in controlling flow through the SCV block. So, we model these intersections as one-dimensional conductors.

The possible high conductivity of secondary fractures in the zones, compared with slickensided fractures in the zones and fractures outside the zones is supported by the results of the numerical example shown in Figure 4.7. We have considered a simplified two dimensional elastic model under far field compressive horizontal and vertical stresses σ_1 and σ_2. According to Chan et al. (1981) and others, the maximum principal in-situ stress is horizontal and has a magnitude of approximately 24 MPa on the 360 m level. This stress is oriented northwest and is therefore perpendicular to the NE-striking zones. The minimum principal stress is vertical and has a magnitude of approximately 9 MPa on the 360 m level. In Figure 4.7a, nine randomly distributed fractures are subjected to these stresses. For simplicity it is assumed that the fractures do not cross each other, and each of these fractures have been given a length of one meter. In Figure 4.7b we look at the same system of fractures, except now two long fractures representing the throughgoing slickensided fractures are added that dip 40°. The long fractures each have a length of 16 m and are separated by 7 m. Thus in Figure 4.7b the nine fractures are subjected to the stress state within one of the NE-striking, low dipping zones i.e. the A, B, B' and C zones.

Due to the application of the in-situ stresses, the modes I and II crack-tip stress intensity factors, K_I and K_{II}, respectively, have been calculated at each of the crack tips utilizing a numerical algorithm based on the work of Kachanov (1987). This algorithm has been modified to account for cracks that are closed by the compressive stresses but can still shear (frictionless surfaces are assumed for closed cracks).

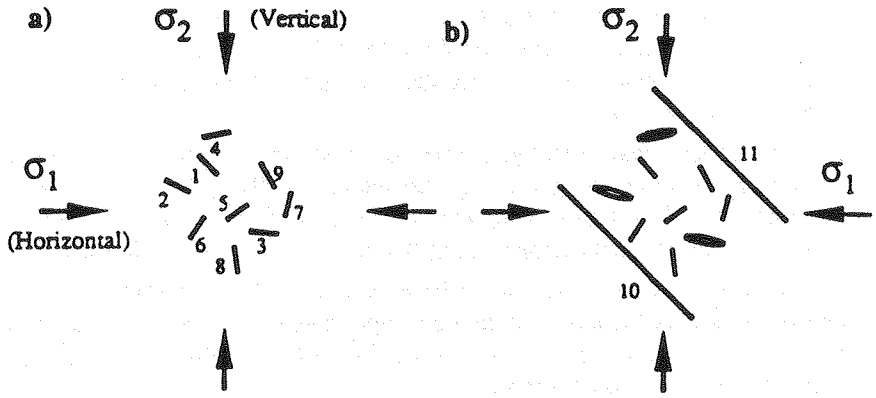

Stress Intensity Factors
(MPa $m^{½}$)

Fracture No.	(a)		(b)	
	K_I	K_{II}	K_I	K_{II}
1	0	-7.8	0	-4.6
2	0	-4.4	0.39	-0.9
3	0	3.7	0	6.1
4	0	5.4	0	9.4
5	0	8.1	0	11.4
6	0	5.9	0	9.70
7	0	2.3	0	5.61
8	0	-4.4	0	-1.4
9	0	-7.5	0	-2.9
10	-	-	0	-29.0
11	-	-	0	-29.0

XBL 896-2393

Figure 4.7. a) Nine randomly distributed fractures subjected to the maximum horizontal and vertical stresses on the 360m level at Stripa, and b) two long fractures representing the slickensided fractures in the NE-striking zones are added. Table lists average Modes I and II stress intensity factors for each crack for the two cases.

The K_I and K_{II} for each crack is presented in the table below Figure 4.7. Each crack has two crack tips, and in Figure 4.7, we only show the average of the two crack tips. K_I is an indication of the opening of the crack, and K_{II} is an indication of the shearing of the crack (Lawn and Wilshaw, 1975). K_{II} can have both negative and positive signs indicating shear in one direction or the other, while K_I can be either positive or zero. $K_I = 0$ indicates that the crack is closed.

Figure 4.7a and 4.7b demonstrate the importance of shear zones in localizing flow in the rock mass. In Figure 4.7a, each of the fractures are under different amounts of shear but they are all closed ($K_I = 0$). In Figure 4.7b, however, due to the localization of shear from the long slickensided fractures, fractures with certain orientations have a positive K_I, and are therefore open. These fractures are sub-horizontal, which agrees with the expected orientations.

Figure 4.7 gives the stress intensity factors for the long fractures, and they remain closed. The sign of K_{II} for the long fractures indicates a reverse dip-slip motion, as the field data suggests for the NE-striking zones. Thus this numerical example supports the idea that the conductivity is greater in dilatant fractures in the zones rather than the main throughgoing fractures that are sub-parallel to the zone.

Figure 4.7 also points out a technical difference between a fault zone and a fracture zone. A fracture zone may contain a high density of fractures, but under compressive far field stresses, the fractures will be closed, as in Figure 4.7a. A fault zone, on the other hand, by containing dilatant fractures, can be more conductive, even if the density of fractures is lower.

In the numerical model, the grid elements are constructed along strike and dip lines. In this way we allow for the horizontal conductors indicated by the geomechanical observations. So, if the geomechanical observations are correct, we expect that fewer of the dip direction elements will be active, i.e. permeable than those in the strike direction.

4.4. SIMULATED ANNEALING

After the conceptual model, or template has been constructed, it must be calibrated such that it behaves like the real rock. In other words, we alter the model using inversion techniques so that the model predicts the observed hydraulic responses. LBL has been developing an inversion technique called "Simulated Annealing" which can be used to construct a system which is functionally equivalent to the observed system: i.e. a model which simulates the same behavior as the observations we have. We describe here how to use annealing to find an equivalent fracture network model. The fracture network model is "annealed" by step-wise modification of the base model, or "template" such that the modified systems behave more and more like the observed system.

Hydrologic inversion models developed in the past, such as the conjugate gradient method, or maximum likelihood method (Carrera and Neuman, 1986) were focussed on determining the conductivity values when the pattern of conductors is known or when everything is well interconnected as in the porous medium case. Annealing could theoretically be used to do this type of inversion, but would be relatively inefficient in this role. On the other hand, these porous medium techniques work poorly when they are asked to completely turn off the conductivity of a portion of the region. Thus they are not the technique of choice for fracture systems when we wish primarily to determine how the conductive features are connected.

Our annealing algorithm is specifically designed to determine an appropriate pattern of conductors among a set of possible configurations. In fracture hydrology, we think that the pattern of conductors is responsible for the first order behavior. In other words, it is most important to know how the system is connected. Annealing is designed to find connections equivalent to those in the field. This is achieved through methodically searching patterns to see which ones behave like the observations in the field. Simulated annealing is actually the statistical technique which controls the acceptance or rejection of trial modifications. The job of simulated annealing is to find near optimal solutions on a complicated function with many possible solutions and local minima.

The set of possible configurations is based on a template or base model which specifies all of the possible connectors. We made the assumption that the behavior is controlled by fracture zones, so we only allow connectors to exist within the zones. This approach has the advantage that it is efficient because it uses the information gained from geophysics and geology *a priori*. A second possible approach is to use a three-dimensional regular grid of conductors as the initial template. This approach has the advantage that the hydrologic responses drive the result more directly but the allocation of conductors may be inefficient.

For either approach, the resolved pattern is not guaranteed to be the same as the one in field, and for this reason we call it an equivalent system. The equivalent systems are non-unique. This means we can find a range of systems which behave the same way the real system behaves. The range of systems can then be used to make a range of predictions and quantify prediction error.

Annealing employs an analogy between optimizing a function with many local minima and the process of annealing a metal to reach its lowest energy state (Kilpatrick, et al., 1983; Tarantola, 1987). Simulated annealing can be viewed as a process of minimizing an energy function over a set of possible configurations of elements. The process of annealing is summarized as follows. In-situ well tests are simulated on the model using TRINET. We then define the "energy," $Q(C)$ of our current model configuration, C, as the squared sum of the differences between the measured and simulated heads, h, taken at a set of locations at discrete time intervals, j:

$$Q(C) = \sum_j [h(o_j) - h(s_j)]^2 \tag{4.1}$$

where

o_j = a vector of observed responses

s_j = a vector of simulated responses

Next we change the model by switching a randomly chosen channel "on" (i.e. conducting) if is it is "off" (i.e. non conducting) or visa versa and then repeat the well test simulation. If the changed model, C', gives simulated well test data closer to the real measured values, i.e. $Q(C)$ is decreased, then the changed model is kept. However, if $Q(C)$ is increased by the change, then the change will be kept with a certain probability, P, which is a function of a weighting factor, T, (called the "temperature"), and $Q(C)$.

At each iteration k, given C, C', and T, the temperature, we can find a matrix of transition probabilities. The probability we will move from configuration C to C', given our current configuration C is equal to the probability that we select C' to compare with C, multiplied by the probability that the system would make the transition to a given C'. That is:

$$P\{C \rightarrow C' \mid C\} = \begin{cases} P(C' \mid C) \cdot 1 & \text{if } C' \neq C \\ & Q(C') - Q(C) \leq 0 \\ P(C' \mid C) \cdot e^{-\left[\frac{Q(C') - Q(C)}{T}\right]} & \text{if } C' \neq C \\ & Q(C') - Q(C) > 0 \end{cases} \tag{4.2}$$

The temperature is decreased as the number of iterations increases to make it more and more unlikely that an unfavorable change will be accepted. At first, a high value of T allows the algorithm to jump up out of local minima and continue searching for a better configuration. Later, lowering the temperature tends to confine the search for a minima, so the algorithm can converge.

At this time, there is a theory which relates the temperature schedule to the convergence properties of annealing. This theory (Hajek, 1988) shows that a temperature schedule which is inversely proportional to the log of the iteration number will converge in probability to a set of minimum energy states, i.e. the optimal configuration. However, a temperature schedule of this type is prohibitively slow. Further, we do not necessarily want to find the minimum energy configuration. We are only interested in finding several good solutions, not in certain convergence in probability to a set of minimum energy states. Therefore, use of Hajek's temperature schedule is over constraining for our purpose.

The temperature schedule we use here is only justified heuristically: it works. We have followed the suggestion of Press, et al. (1986) and decreased the temperature whenever 50 changes have been accepted at the current temperature. Each interval of the schedule with constant temperature is called a step. At the end of each iteration, k, the temperature, T_k, is decreased using a geometric series,

$$T_{k+1} = T_k \, t^k \tag{4.3}$$

where

$$0 < t < 1 .$$

The initial temperature is chosen such that it is of the same order of magnitude as the energy difference between the first two configuration. This is done in an attempt to scale the energy difference between successive configurations to something between zero and one. Other choices of temperature schedule are possible and these are currently the topic of research.

A synthetic example of annealing results is shown in Figure 4.8. Here we have created a synthetic fracture system (Figure 4.8a) and used it to create synthetic well test data. Then, we create a regular grid to use as a template (Figure 4.8b) and apply annealing to find a configuration which matches the synthetic well test data (Figure 4.8c). This example shows that the annealed result roughly reproduces the connection between the wells. Major gaps similar to those in the "real" system have analogous gaps in the annealed system.

A full suite of synthetic cases is being developed to study the effect of template geometry, temperature schedule, weighting functions etc. This suite will give us experience that can be applied to cases where the true geometry is really unknown.

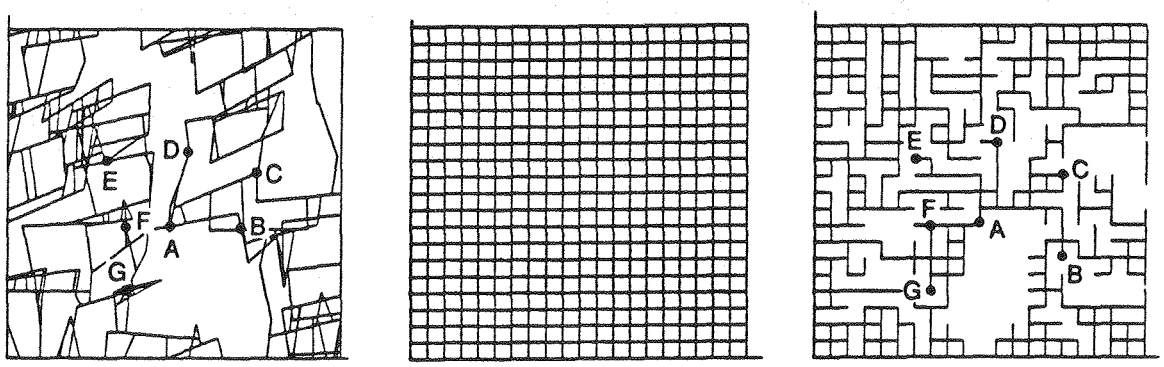

XBL 891-6142

Figure 4.8. a) A synthetic fracture network where we have generated synthetic data on well test in hole A and monitoring in holes B through G; b) template model, and c) the pattern of conductors resulting from annealing.

4.5. PREDICTION OF INFLOW TO THE D-HOLES

At this stage in the hydraulic investigation of the SCV site, there are no formal, well controlled cross-hole well tests available. In order to gain experience with the annealing technique and produce a preliminary estimate of the flow into the D-holes, a synthetic cross-hole test was produced based on a variety of data available for the SCV site. This data consisted of ad hoc cross-hole tests performed by British Geologic Survey (BGS) and the record of heads in the boreholes.

BGS conducted three ad-hoc cross-hole tests by opening W2 and monitoring sections in N3, N4, and W1. Some zones did not respond and some responded very quickly. The test durations were too short to achieve steady-state conditions and the transient data was at best qualitative. However, these tests offer valuable information about the major hydrologic features in comparison to the single hole tests because the scale of these cross-hole tests is much more representative of the overall size of the SCV site and the large hydrologic features.

The transient data do not warrant annealing. However, based on the transient results plus the record of hydraulic heads in the holes, a synthetic steady state test was fabricated. The steady flow rate from W2 was extrapolated to estimated the steady-state flow rate of 10 liters/min. The corresponding estimation of steady state head in N3, N4, and W1 was found by extrapolating the head values in those holes during the period when W2 was opened for prolonged period of time. Wherever possible, these heads were assigned to specific zones in the boreholes based on the responses observed during the ad hoc test. In other words, during the ad hoc tests, the observation holes were divided into several sections. Some sections did not respond to opening W2, whereas others responded very rapidly. In these cases, the responding zone was assigned the observed head.

The annealing case is summarized in Figure 4.9. Figure 4.9 shows the N- and W-boreholes, plus the "fins" that are used to connect the boreholes to the hydrologic zones. Each fin represents the intersection of a zone with the borehole. The black fins are those where we have determined a value of head to use in the calculation of annealing energy based on the ad hoc cross hole tests plus the head record. The gray fins in W2 are held at zero head to simulate the opening of W2. The white fins are those for which we have no record of response to opening W2. Therefore, the value of head at these fins, as well as throughout the network are calculated but not used in the annealing process.

The choice of boundary conditions is based on head observations in the boreholes. The SCV block is situated in a large zone of depressed heads which represent the steady drainage created by the mine. Therefore, whatever perturbations there are in the SCV block must be superimposed on this existing condition. Shut-in heads throughout and around the SCV block are surprisingly consistent and centered about 200m. Therefore we choose the alternative of making the boundary conditions constant head equal to 200m. Although we do not expect the boundary conditions to be uniform around the edges of the zones we have too little data to have any more resolution than setting the boundary conditions to one estimated figure. These boundary conditions do represent a degree of approximation consistent with the rest of the assumptions we have made so far. In order to get a better representation of the hydraulic conditions in the block, we connected each zone to boundaries set at 200 m head far away from the block.

As a starting configuration we randomly removed 20% of the conductors within the block in order to enhance the speed of convergence to a low energy. We expect that annealing will remove many of the conductors in the template in order to match the observed behavior. Making "holes" a priori improves the speed of convergence because if we start with the full grid, the annealing process will turn off every conductor it examines at the early stage anyway. The percentage and the pattern of the starting configuration can be preconditioned using various techniques such as the fractal dimension as mentioned earlier, however, in the present case we chose to do random preconditioning and an arbitrary percentage of 20 instead.

A temperature schedule was chosen as:

$$T_{k+1} = T_k \, 0.7^k \tag{4.4}$$

with

$$T_o = 0.1 \tag{4.5}$$

and the temperature was changed every 20 successful iterations. The annealing program was initiated and continued running for 931 iterations during a period of one week. At that time an inefficient algorithm in the program was detected which was causing the annealing procedure to occasionally retain the previous configuration unnecessarily. This is evidenced in Figure 4.10 between iteration 1 and 931 by the regions on plot where there are two values of energy plotted for the same iteration. At the same time, we found

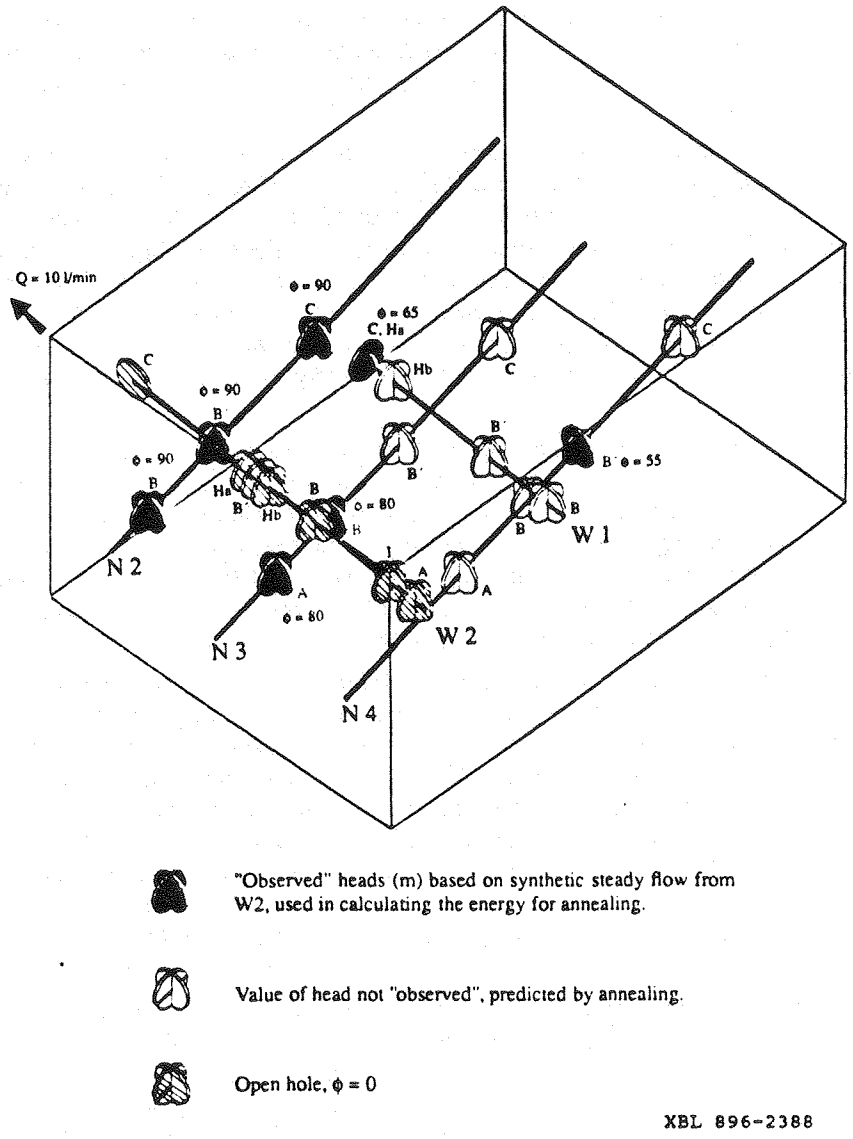

Figure 4.9. Summary of the synthetic well test results used for annealing.

that the head in N3 had been left out of the energy calculation. Hence, the process was stopped and restarted with a refreshed temperature schedule, the current minimum energy fracture configuration, the error corrected, and the fourth well included.

The added well sharply increased the energy level at this point (Figure 4.10, iteration 932). With the process correctly functioning the procedure continued for another five days until the temperature schedule was exhausted and the procedure terminated normally at iteration number 1813. The energy at this iteration was 1.74. To see if we could get the energy closer to zero, the annealing program was restarted with an extended temperature schedule at the current configuration. Also, the annealing program was altered to increase the number of iterations at each temperature from 20 to 50. This change is reflected in the decreased slope of the receding energy function. The process was stopped at iteration number 3749 and energy equal to 0.005661.

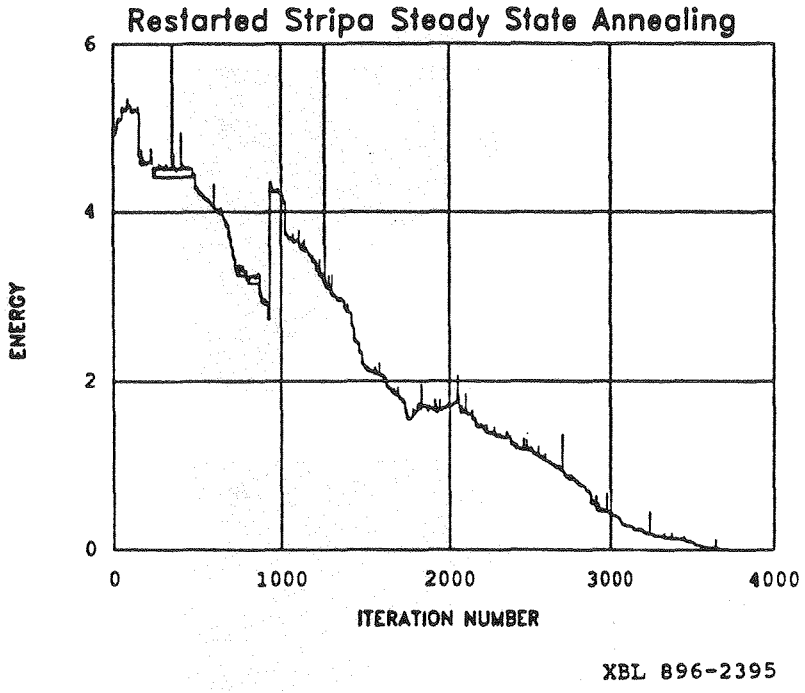

Figure 4.10. Record of energy versus iteration for the SCV synthetic well test case.

Figure 4.11 shows an example configuration of the channels in zone A, including the complete set of possible channels, the initial configuration of channels at the start of annealing, and the configuration of channels at the last iteration. The percentage of elements did not change much from the initial configuration to the final one. We presume that this is because the synthesized annealing case did not contain enough information to warrant changing the percentage. There are some indications that the annealing routine was beginning to find patterns. For example, on zone A, we see that connections between N4 and N3 have become a little sparser after annealing which reflects the fact that zone A responded to W2 in N3 but not in N4. However, none of these changes are very striking and we suspect again that we simply do not yet have enough information to discern the channel pattern.

Table 4.2 gives the heads that were calculated with the final configuration resulting from annealing. We see that the annealing routine has managed to match the observed heads very well. At the end of the annealing process, we have determined several configurations of conductors within the zones all of which result in matching the observed head data extremely well. The match has been achieved solely by arranging the conductors. As all the channels have the same conductance, k_A, any value of k_A will result in the same head distribution.

So, at this point we must calibrate the conductance of the channels such that the model will predict the correct value of flow from W2. To do this, we use the annealed model to calculate the flow from W2, $QW2_A$ with conductances equal to k_A. Then we take the ratio of measured flow to calculated flow to find the conductance of the channels, $kW2$ which would produce the correct amount of flow into W2 ($QW2_M$):

$$kW2 = k_A \cdot \frac{QW2_M l/min}{QW2_A m^3/s} \tag{4.6}$$

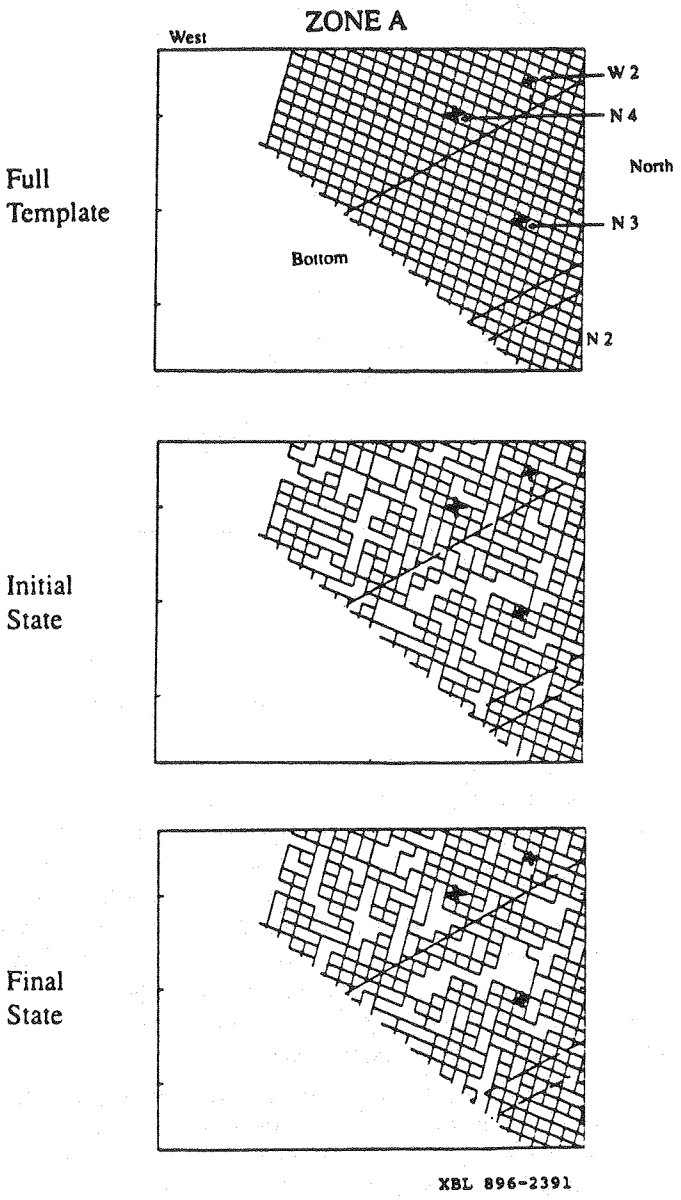

Figure 4.11. Grid elements in zone A. The top is the full template, the middle is the initial configuration, and the bottom is the final configuration after annealing.

For the final configuration of the model, the value of $QW2_A$ is 3.14 m^3/s, and k_A is 0.42 m^3/s, so for the case of $QW2_M$ = 10 l/min, we require that kW2 = 1.34 l/min or 2.2 x $10^{-5} m^3/s$.

Now we rearrange the numerical model, closing the hole W2, and adding the open D-holes and calculating the outflow from the D-holes. We repeat this for seven different configurations of the model. The resulting calculations of inflow to the D-holes are given in Table 4.3. It is clear from these results that the prediction of inflow to the D-holes is largely governed by the measurement of flow from the W2 hole. In fact, by the scaling equation above, the flow into the D-holes is directly proportional to the flow from W2.

Table 4.2. Annealing results at the final iteration = 3749

Hole	Zone	Observed Heads	Predicted Heads
N2	B,B′,C	90	90
N3	A,B	80	79
	B′	none	65
	C	none	65
N4	B′	55	55
	C	none	83
	B	none	49
	A	none	49
W1	H_a,C	65	65
	H_b	none	65
	B′	none	65
	B	none	65

Table 4.3. Inflows to the D-Holes Predicted for Ten Different Configurations of the Model.

Rank of Likelihood	Iteration	Energy	Inflow to the D-holes (l/min)
1	3747	0.005	8.9
2	3568	0.096	9.0
3	2910	0.63	9.1
4	2498	1.32	8.9
5	949	2.94	8.8
6	847	3.13	8.8
7	300	4.62	8.9

This indicates that the prediction of D-hole inflow is extremely sensitive to the measurement of flows. The calculations given in Table 4.3 depend on a single measurement of flow, and we suspect that this measurement is anomalous in that the transmissivity in W2 is much higher than the other holes. This points out that other flow data available for the SCV block would be very useful in modifying this prediction and this is discussed below.

One further set of data is available to aid in the prediction of inflow to the D-holes. This data was also collected, also on an ad hoc basis, by BGS (D. Holmes, personal communication) and consists of measurements of outflows from the other N- and W-holes after they had been left open for periods of time. Table 4.4 gives this data.

First, we note in Table 4.4 that the measured inflow to W2 is 12 l/min. Our best estimate of the steady flow to W2 in 10 l/min, or about 83% of that in Table 4.4. This is because the values in Table 4.4 do not yet reflect steady flow. To correct for this, each of the measurements of flow is reduced by 17%. We call these flows Q_{iM} where i stands for the holes, N2, N3, N4, W1, and W2.

Table 4.4. Open Hole Inflows to N- and W-holes

Hole	Flow (l/min)	Comment
N2	0.60	Measured flow after 6 hours open
N3	0.45	Measured flow after 4 hours open
N4	2.55	Measured flow after 2 hours open
W1	1.30	Measured flow after 2 days of chemical sampling
W2	12.0	Measured flow after 3 hours open

Now, we can use the final annealed configuration of channels with conductance, k_A, to calculate the inflow into each of these holes, Q_{iA}. To do this we simply close W2 by making the nodes at W2 internal nodes, then sequentially open each of the other holes by assigning their nodes zero head. In each case we calibrate the channel conductance in the same manner as previously described such that the model correctly predicts Q_{iM}:

$$k_i = \frac{Q_{iM}}{Q_{iA}} k_A \tag{4.7}$$

This results in five different predictions of channel conductance, which in turn results in five different predictions of D-hole inflow. These predictions are given below in Table 4.5.

Table 4.5. Predictions of D-Hole Inflow Based on Annealing and Measured N- and W-Hole Inflows.

Hole	Measured Flow (l/min)	Adjusted Flow (l/min)	k_i/k_A $\left[\frac{l/m}{m^3/S}\right]$	Predicted D-hole inflow (l/min)
N2	0.60	0.50	0.16	1.3
N3	0.45	0.37	0.12	0.6
N4	2.6	2.1	0.67	3.4
W1	1.3	1.1	0.35	1.3
W2	12.0	10.0	3.2	8.9
Mean	3.4	2.8	.89	3.1
Standard Deviation	4.9	4.1	1.3	3.1

In summary, our prediction of inflow to the D-holes has mean 3.1 l/min and a coefficient of variation (standard deviation divided by the mean) equal to about one. We do not know the form of the inflow distribution function, but if we make a guess that inflows are distributed log-normally, then we can calculate that the flow will be between 0.44 and 11.4 with 95% confidence. Actual measurement of inflow into the D-holes was about 2 l/min.

4.6 SUMMARY OF RESULTS AND CONCLUSIONS

Based on the preliminary data available at this time, the inflow predicted for the D-holes is 3.1 l/m with a standard deviation equal to 3.1l/m. The actual measured value is about 2.0 l/m. The results are most sensitive to the measurements of inflow. We think that this is particularly so due to the fact that the annealing case was so limited and only steady state data was used. Based on synthetic examples, we expect that multiple transient annealing will be able to discern channel patterns much more effectively than steady state annealing. The estimate is sensitive to flow measurements and as it is flow we are predicting, we have confidence that this approach gives answers that make some sense.

Questions remain about weighting some data over others and the effect of different starting configurations of the model. Such a studies are underway using synthetic examples and will include a study of different configurations at the same initial percentage of conductors and well as a study of different percentages of conductors. Along the same lines, we are very interested to try initial configurations that have been conditioned by the fractal analysis. Also, it is not surprising that preliminary synthetic cases show much better resolution of pattern when the template reproduces the orientations of the real conductors. This fact supports the need for the *a priori* definition of the template using geology and geomechanics approaches.

This example should be considered preliminary at best. However, we find the approach very attractive in that the resulting models will contain more information about connectivity than an equivalent continuum model, but are not requiring us to know all the actual details of the geometry. These new models can be considered to be "equivalent lattice models". They reproduce the essential lack of connection prevalent in fracture networks without trying to reproduce every fracture. The modeling effort is concentrated on reproducing the behavior of the observed system rather than the geometry. We think this makes sense because the reason for having a model is to predict behavior, not geometry.

5. References

Barker, J. (1988) 'A Generalized Radial-Flow Model for Pumping Tests in Fractured Rock', Water Resources Research, 24(10), 1796-1804.

Billaux, D., Chiles, J. P., Hestir, K. and Long, J. (1989) 'Three-Dimensional Statistical Modeling of a Fractured Rock Mass - An Example for the Fanay-Augeres Mine', International Journal of Rock Mechanics and Mining Science, special issue on Forced Fluid Flow Through Fractured Rock Masses, in press.

Carlsten, S., Olsson, O., Persson, O. and Sehlstedt, M. (1988) 'Site Characterization and Validation - Monitoring of Head in the Stripa Mine During 1987', SKB Report 88-02, Stockholm, Sweden.

Carrera, J. and Neuman, S. P. (1986) 'Estimation of Aquifer Parameters Under Transient and Steady State Conditions: 2,' Water Resources Research, 22(2).

Chan, T., Guvanasen, V. and Littlestone, N. (1981) 'Numerical Modeling to Assess Possible Influence of the Mine Openings on Far-Field In Situ Stress Measurements at Stripa', Lawrence Berkeley Laboratory, Report No. LBL-12469, Berkeley, California.

Charlaix, E., Guyon, E. and Roux, S. (1986) 'Permeability Effects in the Permeability of Heterogeneous Media, in Fragmentation, Form and Flow in Fractured Media', Annals of Israël Physical Society, 8, 316-324.

Dershowitz, W. (1984) 'Rock Joint Systems', PhD dissertation, M.I.T, Cambridge, Mass.

Englman, R., Gur, Y. and Jaeger, Z. (1983) 'Fluid Flow Through a Crack Network in Rocks', J. Appl. Mech., 50, 707-711.

Kachanov, M. (1987) 'Elastic Solids with Many Crack: A Simple Method of Analysis', Int. J. Solids Structures, 23, 23-43.

Hajek, B. (1988) 'Cooling Schedules for Optimal Annealing', Mathematics of Operations Research, 13(2) 311-329.

Hestir, K. and Long, J. C. S. (1989) 'Analytical Expressions for the Permeability of Random Two-Dimensional Poisson Fracture Networks Based on Percolation and Equivalent Media Theories', submitted to JGR.

Hsieh, P. A., Neuman, S.P., Stiles, G. K. and Simpson, E. S. (1985) 'Field determination of the three-dimensional hydraulic conductivity tensor of anisotropic media: 2. Methodology and application to fractured rocks', WRR 21(11), 1667-1676.

Kachanov, M. (1987) 'Elastic Solids with Many Crack: A Simple Method of Analysis', Int. J. Solids Structures, 23, 23-43.

Karasaki, K., (1988) 'A New Advection-Dispersion Code for Calculating Transport in Fracture Networks', LBL Report, in press.

Kesten, H., (1987) 'Percolation Theory and First-Passage Percolation', The Annals of Probability, 15(4), 1231-1271.

Kilpatrick, S., Gelatt, D. C. and Vecchi, M. P. (1983) 'Optimization by Simulated Annealing', Science, 220.

Kirkpatrick, S. (1973) 'Percolation and Conduction', Reviews of Modern Physics, 45(4), 574-588

Long, J. C. S., Remer, J. S., Wilson, C. R. and Witherspoon, P. A. (1982) 'Porous Media Equivalents for Networks of Discontinuous Fractures', Water Resour. Res., 18(3), 645-658.

Long, J. C. S, (1983) 'Investigation of Equivalent Porous Medium Permeability in Networks of Discontinuous Fractures', Ph.D. Thesis, Univ. Of Calif., Berkeley.

Long, J. C. S. and Witherspoon, P. A. (1985) 'The Relationship of the Degree of Interconnection to Permeability in Fracture Networks', J. of Geophys. Res., 90(B4), 3087-3097.

Long, J. C. S., Karasaki, K., Davey, A., Peterson, J., Landsfeld, M., Kemeny, J. and Martel, S. (1989) 'Preliminary Prediction of Inflow into the D-Holes at the Stripa Mine', Lawrence Berkeley Laboratory report LBL-27182, in preparation.

Olsson, O., Black, J. H., Gale, J. E. and Holmes, D. C. (1988a) 'Site Characterization and Validation, Stage 2 - Preliminary Predictions', Swedish Geological Co. Report ID No. 88.

Olsson, O., Eriksson, J., Falk, L. and Sandberg, E. (1988b) 'Site Characterization and Validation - Borehole Radar Investigations', Stage I, SKB Report 88-03, Stockholm, Sweden.

Orbach, R. (1986) 'Dynamics of Fractal Networks', Science, 231, 814-819.

Press, W. H., Flannery, B. P., Teukolsky, S. A. and Vetterling, W. T. (1986) Numerical Recipes, Cambridge University Press.

Robinson, P, (1984) 'Connectivity, Flow and Transport in Network Models of Fractured Media', PhD Dissertation, St. Catherine's College, Oxford

Sen, P. N, Scala, C. and Cohen, M. H. (1981) 'A Self Similar Model for Sedimentary Rocks with Application to the Dielectric Constant of Fused Glass Beads', Geophysics, 46(5), 781-795.

Snow, D. T. (1965) 'A parallel plate model of fractured permeable media', Ph.D. dissertation, 331 pp., Univ. of Calif., Berkeley.

Snow, D. T. (1969) 'Anisotropic permeability of fractured media', Water Resour. Res., 5(6), 1273-1289.

Tarantola, A. (1987) Inverse Problem Theory, Elsevier Science Publishing Company Inc., New York, N.Y.

6. Acknowledgements

This work was supported by the Manager, Chicago Operations, Repository and Technology Program, of the U.S. Department of Energy, under Contract No. DE-AC03-76SF00098. The authors are also grateful to the Stripa Project and the French Bureau de Recherches Geologiques et Minières, M. Daniel Billaux in particular. For their thoughtful reviews, we would like to thank Professors Kunal Ghosh and Paul A. Witherspoon. For typing, graphics and the removal of inconsistencies, we thank Ellen Klahn and Diana Parks. Finally, the senior author praises "the team".